Numerical Prediction of Hydrodynamic Characteristics of Modern Marine Propulsive Device in Steady Flow

by

Mohammad Kamrul Hasan
Roll No: 040409003F, Registration No: 0404393
Session: April 2004

**MASTER OF PHILOSOPHY
IN
MATHEMATICS**

Department of Mathematics
**BANGLADESH UNIVERSITY OF ENGINEERING AND
TECHNOLOGY, DHAKA.**

March.2009

#107232#

The Thesis entitled

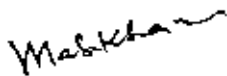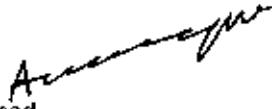# Numerical Prediction of Hydrodynamic Characteristics of Modern Marine Propulsive Device in Steady Flow
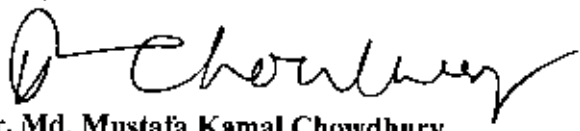
Submitted by
Mohammad Kamrul Hasan

Roll No: 040409003F, Registration No: 0404393. Session: April 2004, a full time student

of M. Phil (Mathematics) has been accepted as satisfactory in partial fulfillment for the

degree of

MASTER OF PHILOSOPHY IN MATHEMATICS

March 21, 2009

Board of Examiners
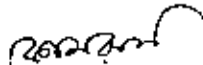
(i) **Dr. Md. Abdul Hakim Khan**   (Supervisor)   Chairman
   Professor
   Department of Mathematics
   BUET, Dhaka-1000.

(ii) **Dr. Md. Mashud Karim**   (Co-Supervisor)   Member
   Associate Professor
   Department of Naval Architecture & Marine Engineering
   BUET, Dhaka-1000

(iii) **Head**   (Ex-Officio)   Member
   Department of Mathematics
   BUET, Dhaka-1000

(iv) **Dr. Md. Mustafa Kamal Chowdhury**   Member
   Professor
   Department of Mathematics
   BUET, Dhaka-1000.

(v) **Dr. Md. Refayet Ullah**   Member (External)
   Professor
   Department of Naval Architecture & Marine Engineering
   BUET, Dhaka-1000

Author's Declaration

I declare that the work done in this dissertation is followed in accordance with the regulations of Bangladesh University of Engineering and Technology, Dhaka. I also declare that this is an authentic record of my own work except where indicated by special reference in the text. No part of this text has been submitted for any other degree or diploma.

The dissertation has not been presented to any other university for examination either in Bangladesh or overseas.

Date:

Mohammad Kamrul Hasan

Acknowledgements

Abstract

A potential based Surface Panel Method (SPM) is applied to the hydrodynamic analysis of modern marine propusive device, i.e., podded propulsion system (PPS) in steady flow. At first the surface of the body is approximated by a number of small hyperboloidal quadrilateral panels with constant sources and doublet distributions. The surface of the trailing vortex sheet is also represented by hyperboloidal quadrilateral panels with constant doublet distributions. The strengths of source and doublet are determined by solving the boundary value problem at control point of each panel surface satisfying some boundary conditions. Effect of viscosity is incorporated to the potential solution using Prandtl-Schlicting formula. The method is first applied to analyze pod, strut and propeller separately, then the combination of pod-strut geometry and finally the complete pod propulsion system, PPS (Propeller + Pod + Strut).

Appling this method, the pressure distribution on the pod and strut used in podded propeller system are determined and compared with published results. The method is also used to evaluate effects of hub taper angle and pod-strut geometry on the open water characteristics of a fixed pitch screw propeller used in podded propulsion system in pusher configuration. The method is validated by comparing the predicted results with experimental measurements.

Effects of hub taper angle on hydrodynamic characteristics are studied numerically in terms of thrust coefficient, torque coefficient, and propulsive efficiency for a wide range of advance coefficient in case of hub taper angles of 0°, 5°, 10°, 15°, 20° and 25° in pusher configuration. The effect of pod-strut geometry on the hydrodynamic

characteristics of tapered fixed pitch screw propellers used in pusher podded propulsion systems has also been studied numerically. Different pod-strut configurations are modeled for tapered hub propellers with hub taper angles of $0°$, $5°$, $10°$, $15°$, $20°$ and $25°$ respectively. In this case, only the characteristics of the propeller are predicted in presence of pod-strut geometry (propeller with pod-strut). In other word, blockage effect due to the presence of pod-strut body is taken into account ignoring the losses due to skin friction imposed by that body.

Major findings include well agreement of results predicted by the method with measurement, significant effects of hub taper angle on hydrodynamic characteristics of propellers, considerable increase in hydrodynamic characteristics of propeller when pod-strut body is attached forward to it in pusher configuration.

Table of Contents

List of Tables

List of Figures

Nomenclature

C_P	Pressure coefficient
D	Propeller diameter (m)
D_{ij}	Influence coefficients due to dipoles on body
G	Green function
J	Advance coefficient
K	Number of propeller blade
K_T	Thrust coefficient (N)
K_Q	Torque coefficient (N.m)
$\boldsymbol{n}$	Unit normal vector
n	Revolution per minute
N_C	Number of chord-wise panels
N_R	Number of radial panels
p	Pressure on the body (N/m^2)
$p(x, y, z)$	Field point
P_∞	Pressure at infinity (N/m^2)
P/D	Pitch ratio
$q(\xi, \eta, \zeta)$	Boundary point
Q	Total torque (N.m)
Q_F	Frictional component of torque (N.m)
r_h	Boss or Hub radius
R	Propeller radius
$R(p;q)$	Distance between p and q
Re	Reynolds number
S_B	Boundary surface
S_W	Wake surface
S_{ij}	Influence coefficients due to source
T	Propeller thrust (N)
T_F	Frictional component of thrust (N)

V_A	Velocity of advance (m/s)
V_I	Inflow velocity (m/s)
W_{ij}	Influence coefficients due to dipole on wake
ϕ	Perturbation potential
η	Propulsive efficiency
ν	Kinematic viscosity (m^2/s)
ρ	Fluid density (kg/m^3)

Acronyms

BEM	Boundary Element Method
CFD	Computational Fluid Dynamics
CP	Conventional Propeller
DARPA	Defense Advanced Research Projects Agency
DAT	Double Acting Tankers
DTRC	David Tailor Research Centre
DTMB	David Tailor Model Basin
FVM	Finite Volume Method
NACA	National Advisory Committee for Aeronautics
PPS	Podded Propulsion System
QVLM	Quasi Vortex Lattice Method
RANSE	Reynolds Averaged Navier-Stokes Equations
SRI	Ship Research Institute
VLM	Vortex Lattice Method

CHAPTER 1

1. INTRODUCTION

1.1 Background

Over the last decade, a new type of propulsion named "podded propulsion" is becoming increasingly popular as an alternative to "conventional" diesel-mechanical or diesel-electrical propulsion especially in cruise ships. A synergy of present day concept of azimuthing thruster propulsion and maneuvering, diesel electric propulsion along with important hydrodynamic aspects, automation systems, etc. finally resulted in a brilliant idea of including an electric motor inside the thruster hub driving the propeller directly, which is now commonly known as "podded propulsion". Thus the "pod" concept eliminates reduction gears, driving shafts, support bearings, stern tubes and finally rudders if azimuthing pods are used. The major advantage of these units over conventional propeller based system is their ability to provide thrust in all directions, giving high maneuverability and good sea-keeping. Due to the above-mentioned key benefits along with some other associated advantages, pods are also receiving increased attention for other types of ships like tankers, ice-going vessels, supply vessels, semi-submersibles etc. Even for naval ships where the concept of "all electric ship" is gaining popularity, podded propulsors remain as the only solution. Podded propulsion is also being seen as an option for increasing existing power, i.e., speed or as replacement for conventional azimuthing thrusters for better station keeping dynamic positioning capability. Despite these advantages, podded propulsion systems have some disadvantages, such as high capital cost, bearing failure and some other structure problems. Basically, two types of pod propulsion systems are used in the marine industry, namely, pusher pod propulsion system and puller pod propulsion system. In a pusher pod

propulsion system, the propeller is attached to the after end of the pod, so that the propeller pushes the unit. On the other hand, in a puller (also termed as tractor) pod propulsion system, the propeller is attached to the fore end of the pod, so that the propeller pulls the unit.

Since ships with pods register acceptable performances, an extensive amount of research work has been carried out both experimentally and theoretically to evaluate hydrodynamic characteristics of podded propulsion system. However, more investigations are underway and still require to be established for better computational techniques satisfying full-scale performance in the field of resistance, propulsion and especially in maneuvering. Operating experiences and their continuous feedback to manufacturers and research establishments are key elements for further improvement on pod design and their construction for future ships of various types and sizes.

Naval architects, marine engineers, hydrodynamicist, mathematician, ship owners and manufacturers have to work together to accomplish an ultimate goal of safe, reliable and comfortable ship to operate. Still a lot of new challenges exist because of future wider applications of pods as modern marine propulsive devices. However, they need to be dealt with careful research, planning and implementation.

1.2 Objective of this Research

The main objective of this research work is to analyze pod propulsion system for determining pressure distribution and the magnitude of hydrodynamic forces on the propulsor of known geometry and known operational parameters. Finally the effects of

2

hub taper angle and pod-strut geometry on hydrodynamic characteristics of podded propellers in pusher configuration are also studied.

The following steps are applied to achieve the objectives:

-To review previous research work and collect data for geometry of podded propulsion system, i.e., size of the pod and strut, propeller diameter and its pitch distribution, maximum thickness and camber distribution, rake distribution, skew distribution and sectional data of the propeller blade, i.e., chordwise thickness and camber distributions and collect also published numerical/experimental results.

-To model the bodies with a number of hyperboloid quadrilateral panels.

-To develop and extend a computer programs to analyze the bodies using surface panel method considering steady potential flow around it.

-To compute velocity and pressure distributions on the body.

-To compute hydrodynamic characteristics, i.e., thrust, torque and performance of the propeller.

- To add viscous effect to the potential solution.

- To validate predicted results comparing with published experimental values.

-To investigate the effect of hub taper angle and pod-strut geometry on the hydrodynamic characteristics of the podded propulsion system.

1.2.1 Effects of Hub Taper Angle

To streamline the pod profile, the hub of the propeller can be tapered at a certain angle. That is, a more conically shaped hub is usually used for a podded propeller, rather than the straighter or cylindrical hub used in conventional fixed pitch propellers. Hub taper angle is usually measured at the blade root section about the geometric center of the

3

propeller. Positive hub taper angle is used for push podded propeller configurations and it reduces the diameter of the straight hub in downstream direction. Negative hub taper angle reduces the hub diameter in the upstream direction and is used in puller propeller configurations. A numerical study of effects of hub taper angle on hydrodynamic characteristics of the model propeller is done in terms of propeller open water characteristics, namely thrust coefficient, K_T, torque coefficient, K_Q, and propulsive efficiency, η, versus advance coefficient, J. The calculations are done for hub taper angles of $0°$, $5°$, $10°$, $15°$, $20°$ and $25°$.

1.2.2 Effect of Pod-Strut Geometry

In a push type podded propulsion system, the pod-strut body stays forward of propeller while operating in normal operating mode. Due to the presence of the pod-strut body forward of the propeller, the flow field (operating environment) around the propeller changes, which affects the hydrodynamic performance of the propeller. The prediction of the effects of the presence of the pod-strut body in push configuration on hydrodynamic characteristics of the propeller is performed in this research work. Another numerical study has been performed on the effect of pod-strut geometry on hydrodynamic characteristics of tapered fixed pitch propellers used in pusher mode. This study has also been done in terms of thrust coefficient, K_r, torque coefficient, K_Q, and propulsive efficiency, η, for a wide range of advance coefficient, J, for six pod-strut configurations, namely PS H0, PS H5, PS H10, PS H15, PS H20 and PS H25. In this case, only the performance of the propellers is predicted, not the performance of the whole units (propeller with pod-strut)

CHAPTER 2

2. REVIEW OF RELATED WORK

A review of podded propulsion systems is the primary focus of this chapter. A brief summary of the major experimental and numerical work which have been performed on podded propulsors since the introduction of this propulsion arrangement is then presented.

2.1 Podded Propulsion System

The podded propulsion system is a modern ship propulsion concept. A podded propulsor defined as a pod housing an electric motor, which drives an external propeller. In the podded propulsion system, the arrangement of the traditional propulsion system (i.e., a propeller mounted at the after end of a long shaft supported by struts and a rudder mounted aft of the propeller) is essentially modified. For a podded propulsor, a fixed pitch screw propeller is fitted at the fore/aft end of an azimuthing pod (generally a body of revolution big enough to enclose an electric drive and other relatively smaller accessories) located at the ship's stern. An electrical motor located inside the pod drives the propeller through a short shaft. The pod is attached to the ship hull by a streamlined strut and a slewing bearing arrangement, both of which have azimuthing capability; thus the whole pod-strut structure can rotate 360°. The thrust produced by the propeller can be directed in any horizontal direction, thus eliminating the need for a rudder. The prime movers/generators are usually located topside of the strut or elsewhere in the ship, requiring only electric cable to the pod. A pair of podded propulsor systems is shown in Figure 2.1 and a schematic view of the major components of a typical podded propulsion

5

system is shown in Figure 2.2.
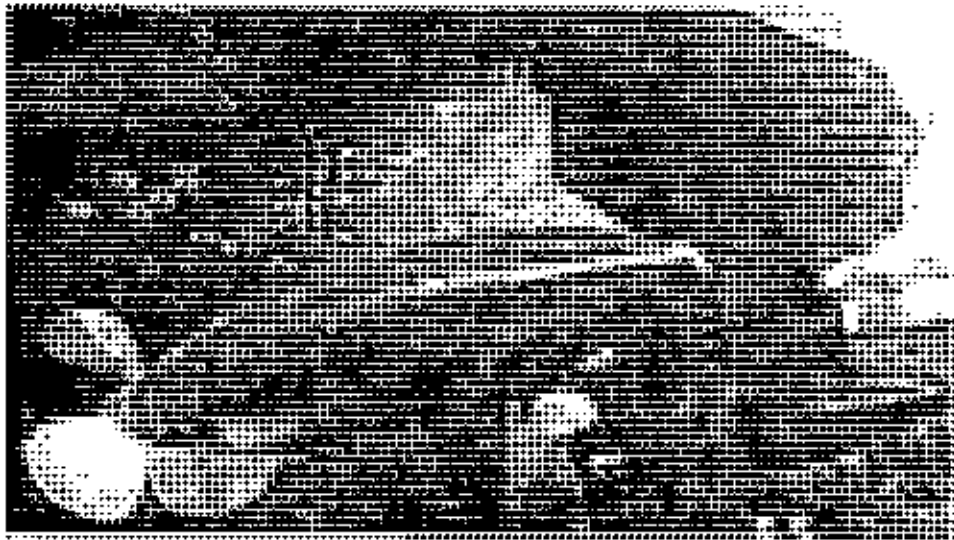
Figure 2.1: A pair of podded propulsor system under a hull.
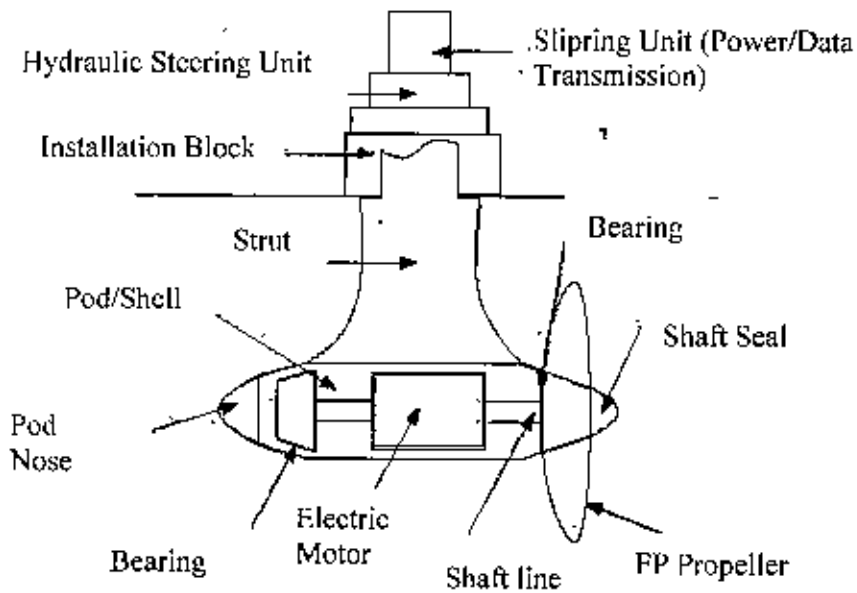
Figure 2.2: A schematic diagram of podded propulsors showing its major components.

Basically, two types of pod propulsion systems are used in the marine industry, namely.

pusher pod propulsion system and puller pod propulsion system. In a pusher pod propulsion system, the propeller is attached to the after end of the pod, thus the propeller pushes the unit. In a puller (also termed as tractor) pod propulsion system the propeller is attached to the fore end of the pod, thus the propeller pulls the unit.

The use of a mechanical azimuthing pod system with the engine connected to a propeller through shafts and mechanical coupling has been widely used, especially for its outstanding manoeuvring qualities. However, the use is limited to relatively small vessels due to limitations in installed power. The idea of placing an electric engine inside the pod shell solved the problem of delivered power, making the new system attractive for big cruise ships, large tankers, ice breakers and ferries with diesel electric propulsion. The pod propulsion systems have proven to be a very attractive alternative propulsion system for ship owners (especially for large commercial vessels). The reason for this may be due to the fact that this propulsion system offers enhanced hydrodynamic efficiency and improved manoeuvering performance.

2.2 Advantages of Podded Propulsion Systems

The advantages of azimuthing-podded propulsor are numerous both from a structural and hydrodynamic point of view. It offers both shipyard/construction benefits and owner/operator benefits. In addition to several advantages offered by electric propulsion in general, vessels built with propulsion pods have several advantages over their mechanical gear, shafted propulsion counterparts. A general discussion on various advantages is presented as follows:

7

2.2.1 Structural benefits

Simple hull form: The entire pod body hangs underneath a ship's stern, thus reducing machinery space required in hull. The removal of long shafting, bearing and reduction gears reduces the hull volume required for podded propulsion machinery resulting in simpler hull form, which ultimately increase cargo space (reduced vessel size) [Trouwborst, 1998 ; Lavini, 1990 and Lepeix, 2001].

Easy installation and maintenance: Main machinery is accessible for removal and replacement. Installation and replacement of pods can be quicker and simpler than that of conventional shafting. The pod can be fabricated and tested in a shop and installed as a module; whereas conventional shafting requires alignment and components inside the hull. While shaft seals are required for each of the bulkhead and hull penetrations in conventional shafting, a podded propulsor requires only the gland seals in the pod [Trouwborst, 1998].

Increased survivability in case of structural damage. [Trouwborst, 1998]

Reduced construction cost: The elimination of the mechanical components reduces shipyard/supplier coordination work. Simplified stern shape reduces building costs [Trouwborst, 1998 and Nocod and Simon, 1998].

2.2.2 Hydrodynamic benefits

Improved power/speed curve: The power/speed curve is improved, due to the absence of appendages: rudders, shafts, brackets, and aft lateral thrusters. The additional power required to overcome pod resistance is only a portion of that saved due to the removal of conventional appendages. The final improvement is not yet easy to predict, but is

8

sufficient for considering pods as an attractive solution especially for larger vessels [Laukia, 1996 and Trouwborst, 1998].

Improved cavitation performance: In a tractor/puller pod propeller the flow is more uniform than it is with a pusher pod or conventional shaft propeller resulting in maximized cavitation free forward speed (lower wake variations in inflow to propeller). The propeller in puller mode can be axially aligned with the inflow to minimize inflow angle variation to the propeller blade. The resulting advantages are decreased unsteady forces, decreased vibrations, decreased circumferential variations in blade loading and inflow velocity, resulting in improved cavitation performance with regard to inception speed, extent of cavitation, and cavitation related erosion [Rains and Vanlandingham, 1981 ; Raynor, 1998 ; Pustoshny and Kaprantsev . 2001].

Potential of quietness: Another advantage is its potential for quietness. The gear noise is avoided by using an electric motor. Reversal of propeller rotation is achieved either by using switchgear or by rotating the entire pod unit through 180°, enabling a fixed-pitch propeller to be used and thus eliminating the hydraulic noise and large hub associated with controllable pitch propellers. The reduction of cavitation also reduces cavitation related noise [Triantafyllou et al., 2003]

Lower appendage drag: Appendage drag is reduced by replacing open shafts and multiple struts with pods and a single strut. Thrust developed by the propellers can be directed anywhere within a 360° compass because of the azimuthing capabilities of the whole unit. Rudder and skegs may be removed, which results in lower appendage drag [Triantafyllou et al., 2003].

Better hydrodynamic performance: Provided that the same hull form is used, the propulsive performance of a podded propulsion system diminishes a little when used in place of a conventional propeller rudder arrangement (because of the additional resistance

9

of the pod-strut bodies). But when a podded propulsor is used as the main propulsion unit of a vessel, an improved buttock flow stern shape with lower hull resistance can be fitted, which leads to excellent inflow characteristics and small cavitation extents on the propeller blades. These lead to better overall performance of the propulsion unit. Design flexibility about the location of the engine room and exclusion of long shaft line and brackets also lead to improved arrangement and hull efficiency [Mewis, 2001 and Triantafyllou et al., 2003].

Better manoeuvring performance: Substantial improvement of manoeuvrability is achieved when a podded propulsion system is used. The crash stop distance is almost half the distance of a open shaft propeller of similar arrangement and the vessel remains maneuverable during crash stop [Toxopeus and Loeff, 2002]. The steering capabilities is significantly greater than with conventional rudder system and thus any stern thruster needed with a conventional propulsion can be eliminated.

Propulsion redundancy: In contra-rotating podded propulsion systems, propulsion redundancy is achieved with two independently operating propellers [Triantafyllou et al., 2003]

2.2.3 Benefits related to electric propulsion

Reduced total installed power generation [Triantafyllou et al., 2003]

Reduced total fuel consumption and exhaust emissions: High fuel efficiency because the prime movers, most often medium speed engines, can run at optimum power [Triantafyllou et al., 2003]

More environment friendly: This propulsion system is more environment friendly there is practically no risk of oil leakage [Triantafyllou et al.. 2003].

10

The flexibility and economy of multipower level operation [Triantafyllou et al., 2003].

Simple and reliable reversible capability [Triantafyllou et al.. 2003].

Flexible operation over a whole rpm range, thanks to roller bearing [Triantafyllou et al.. 2003]

High power density and small size of components [Triantafyllou et al., 2003]

Simple fixed pitch propeller is used: Instead of controllable pitch propellers, more reliable fixed pitch propellers can be used. An electric motor can operate at zero number of revolution hence fixed pitch propeller can be used at low sail speeds [Triantafyllou et al., 2003].

Less noise and vibration: Generators can be placed at remote position, where they produce least noise and vibrations. This is very easy because no mechanical links exists between prime movers and propulsion [Rains and Vanlandingham, 1981 and Terwisga et al., 2001].

Podded propulsion looks more attractive especially for diesel electric twin screw vessels fitted with pulling propellers. It has been shown that for this case a better hydrodynamic performance. better maneuverability and higher comfort standard on board can be achieved [Lavini, 1990]. It certainly opens a possibility of an innovative ship stern design with respect to ship resistance.

2.3 Disadvantages of Podded Propulsion Systems

The podded propulsion system has brought with it some structural and hydrodynamic drawbacks. A recent study [Carlton. 2002] found that the sources of failure on podded propulsors are mainly due to failure of bearings, seals, electric, cavitation, grounding and

shafting. The main disadvantages of a podded propulsion system are summarized as follows:

2.3.1 Structural disadvantages

More exposure to damage: The drive motor is more exposed to damage from grounding or collision [Triantafyllou et al., 2003]

Difficulty in maintenance: The drive motors are less accessible from inside the hull, so maintenance is more difficult [Triantafyllou et al., 2003].

Insufficient lubrication to the bearings [Triantafyllou et al., 2003].

Structural risks of fatigue failure and vibration of a heavy unit suspended on a strut [Carlton. 2002].

High investment cost [Triantafyllou et al., 2003]

2.3.2 Hydrodynamic disadvantages

Increased drag: Increased drag because of pod [Triantafyllou et al., 2003].

Reduced course keeping ability: A design consequence of the application of pods is that freedom is obtained to design a very flat aft ship, which is often favorable from a resistance point of view, and creates a very homogeneous flow towards the pods. The open aft ship possesses little lateral resistance; hence the course keeping ability will be small, especially for single unit installations. In general, the podded ships are more course unstable than conventional ships [Terwisga et al., 2001].

Large heel angle: Large heel angle occurs in ships with podded drive while turning. The

12

pods are very powerful steering tools. The side force that can be generated is so large that the steered vessel can suffer from very large heel angles [Terwisga et al., 2001].

Excessive roll: Excessive roll occurs due to smaller lateral force available in the hull [Toxopeus and Loeff, 2002].

Necessity of operating a heavy unit: Necessity of operating a heavy unit even for a minor course change and course keeping [Toxopeus and Loeff, 2002].

Detailed design work: The design details may need refinement and pod and aft hull configurations must be fully integrated and optimized [Terwisga et al., 2001].

2.3.3 Bearing problems

Among many problems that faced in operations with podded propulsors, the bearing problem is the one, which has given most trouble.

• Thrust bearings operate in a confined space inside the pod body and the dissipating heat has led to some difficulties [Carlton, 2002].

• Radial bearings (slewing and shaft bearings) have to sustain perpetual movements as the vessel maintains a course, while dealing with the lateral thrust from the whole unit hanging beneath the hull. These require the bearing to be manufactured with high order engineering precision [Carlton, 2002].

The main problems for a podded propulsor are the dimensions and weight of the electric motor, the speed control of it and the bearing and sealing problems. Until recently the power density of the electric motors is insufficient resulting in large and heavy electric motors for relatively small powers.

13

2.4 On Podded Propulsion Systems

The podded propeller arrangement is initially used in icebreaking cargo ships. Its application has extended to large cruise ships, tankers, cruisers and high speed research vessels. The technological knowledge level on this arrangement lags behind its practical applications. Although a good number of model and full-scale tests, and some numerical work have been done to enhance the knowledge, there are still knowledge gaps, especially in the understanding of their hydrodynamics. While azimuthing propulsion in the form of low-power electric, hydraulic, or right angle gear-driven steerable thrusters has been around in the practical field for nearly half a century, it has been only in the last decade that electric motor technology has advanced to the point where implementation of high-power azimuthing electric-drive propulsors has become practical for primary propulsion [[Triantafyllou et al., 2003]. In the 1960's, the pod propulsion systems (that housed a right angle mechanical drive system to power the propeller) are used for the first time. The main application of those early strut-pod systems is to provide propulsion to hydrofoil ships where the entire strut, pod and hydrofoil could be retracted out of water [Karafiath and Lyons, 1998].

2.4.1 Experimental Work on Podded Propulsion Systems

Hydrodynamic model tests are conducted on some fixed (non-azimuthing) pods, in which a large pod with propeller is fixed to the hull and a rudder at the trailing edge of the hull provided for steering in the 1950's [Karafiath and Lyons, 1998]. These studies are done on several design concepts with the goal of improving propeller cavitation and powering for an escort type ship. An early but detailed investigation into some

14

hydrodynamic issues such as pod-strut total drag and full-scale power prediction of vessels fitted with podded propulsors (not azimuthing) is done by Rains and Vanlandingham (1981).

Halstensen and Leivdal (1990) discussed various hydrodynamic and mechanical aspects of a tractor type podded propulsion system SPEEDZ. Several model tests and full-scale measurements of this high-speed craft propulsion system are discussed and the system is recommended as a promising alternative for speeds up to 50 knots. Chen and Tseng (1995) presented a design procedure of a contra-rotating propeller with a tractor pod for a high-speed patrol boat and measurements of power and cavitation behavior. Laukia (1996) discussed various hydrodynamic issues related to the design and use of a commercial azimuthing podded drive Azipod. Niini (1997) performed a similar study and discussed various hydrodynamic aspects of Azipod, especially from efficiency and manoeuvrability points of view as applied to large cruise ships.

Kurimo (1998) presented sea trial results on general hydrodynamic issues such as speed trials, cavitation observation, pressure pulse measurement and manoeuvring tests. Facinelli and Muggeridge (1998) presented an integrated system analysis consisting of a mathematical model for costs and performance of the main components of podded propulsion for surface combatants for the US Navy. Karafiath and Lyons (1998) presented a summary of analyzed results of model experiments on powering performance and other hydrodynamic characteristics of pod propulsion done by the US Navy over a period of 20 years. The authors also discussed several hydrodynamic issues. Raynor (1998) discussed the prospects, design issues and some manoeuvring characteristics of podded propulsion in the offshore market especially for monohull and semi-submersibles.

15

Nocod and Simon (1998) discussed the configuration and special benefits of using the commercial electric propulsion system Mermaid[TM]. Kron and Holmstrom (1999) presented extensive model test results regarding propulsive performance, cavitation and pressure pulse performance on Mermaid[TM] propulsion system. The paper also gives a comparison between model tests and CFD calculations and also between a conventional propeller arrangement with rudder and the Mermaid[TM] propulsion system.

Bose et al. (1999) briefly discussed general power extrapolation methods and test procedures for podded propulsors. Karafiath and Lyons (1999) presented detailed measurements and analyses of tests conducted with a view to have better understanding on the hydrodynamic characteristics of podded propeller concepts as applied to fast naval vessels.

Backlund and Kuuskoski (2000) discussed various design features and benefits of using a contra-rotating propeller with a podded drive, demonstrated with a case study. Lavini (1990) provided some guidelines for hull design for twin screw ships with podded propulsors. The author also presented some sea trial results of existing ships with new podded propulsors and a propeller design procedure for podded propulsors. Pustoshny and Kaprantsev (2001) presented results of observations of full-scale propeller blade cavitation patterns carried out on the passenger ship *Elation*, equipped with AZIPODS. Lepeix (2001) discussed different hydrodynamic issues such as power/speed curve, ship wake and pressure fluctuation and manoeuvring performance of large cruise ships with podded propulsors and discussed the new trends in hull lines of large podded driven cruise ships. Terwisga et al. (2001) discussed some critical hydrodynamic issues and design consequences of several steerable thrusters and podded propulsors and put them in

16

an historic perspective.

Mewis (2001) described model tests procedures and presented the results obtained on podded propulsors giving the effects of the presence of pods and propeller gap pressure on the propulsive efficiency of the pod unit. Carlton (2002) presented some design and service experience of podded propulsors while discussing some critical issues related to failure of the propulsors. The author also provided a case study to demonstrate various causes of failure of pods and their possible solutions. Kim and Choi (2002) investigated powering performance of three different propulsion systems for ultra-large container vessels through various model tests and concluded that the contra-rotating azimuthing podded propulsor is a serious alternative. Toxopeus and Loeff (2002) presented various aspects of application of pods from a manoeuvring viewpoint, comparing the manoeuvrability between a ship designed with conventional propulsion and pod propulsion and highlighted the benefits and points of attention of using pod propulsion.

Trägärdh et al. (2004) presented the results of model tests and sea trials done on Double Acting Tankers (DAT) showing good propulsive, manoeuvring and cavitation performance. Triantafyllou et al. (2003) presented some preliminery results of experimental investigation of propulsor induced manoeuvring forces and moments of podded propulsor,with emphasis on the application to nonlinear vehicle maneuvering dynamics.

2.4.2 Numerical Work on Podded Propulsion Systems

While considerable experimental work has been performed on podded propulsion over

17

the last two decades, there is relatively little work on the hydrodynamic performance using numerical methods, such as panel methods and viscous flow method. The numerical methods used to model and predict the performance is primarily the panel method. An early application of the potential flow method to predict the hydrodynamic performance of hull forms with podded propulsors is presented by Cheng et al. (1989). The authors used a free surface potential flow method to generate a complex model for tractor-type podded propulsors appended to a 154-foot transom stern research vessel, *R/V* Athena and computed the flow field around the hull and the appendages. The steady flow induced by the propulsor is simulated by an idealized propeller model (actuator disk) based on Rankine's momentum theory of propeller action. Interactive graphics are used in conjunction with preprocessors and postprocessors to verify the geometric data and to visualize the computed flow field around the hull. The flow visualization is used to examine the proper alignment of the pod/strut system with the aim of obtaining the optimal flow into the propeller. Computational results are given at design speed for two arrangements of pod-strut systems: with and without the actuator disk (to approximately represent a propeller) to examine the upstream effects of the actuator disk. The predictions of the three components of local velocity as presented in vector and contour plots in the propeller plane agree well with the measurements. Harmonic analyses of the propeller inflow in the presence of the pod-strut are performed and the absence of any higher order harmonics in the velocity components confirmed the fact that the podded propulsion produces a more uniform propeller inflow and improves propeller performance.

Kawakita et al. (1994) presented a surface panel method to analyze the hydrodynamic performance of a hydrofoil system consisting of hydrofoil, strut and pod configuration.

They used a low order potential-based surface panel method in which the hydrofoil, strut and pod are represented by hyperboloidal quadrilateral panels with a constant source and doublet distribution and the trailing vortex wake is also represented by hyperboloidal panels with a constant doublet distribution. Free surface effect is taken into consideration by introducing the negative image of the bodies. A Newton-Raphson iterative method is adopted to solve the nonlinear functions resulting from the Kutta condition of equal pressure on the upper and lower surfaces at the trailing edge. The velocity distribution, pressure distribution, lift coeffcient and cavitation number are calculated using standard formulations. Validation of the code is done against measurements done in the towing tank and cavitation tunnel at Nagasaki Experimental Tank.

Szantyr (2001) presented a surface panel method calculation of hydrodynamic analysis of podded propulsor performance with validations. A low order quadrilateral flat panels with constant distribution of dipole strength over the propulsor system consisting of two propellers, pod, strut, two side winglets and duct around the back propeller is used. Similar distribution is used over the wake too. Interaction effects between different rotating and non-rotating elements of the system are taken in to account in simplified form. The resulting solution of potential flow around the propulsor is supplemented with the calculation of parameters of viscous wake behind stationary elements of the propulsors based on simple semi-empirical formulations. The velocity and pressure distribution and the resulting hydrodynamic forces on the pod propulsor of known geometry at given operating condition are predicted. Good agreements of the predicted hydrodynamic forces with measurements are found especially for the axial force component. No prediction is made on the propulsive characteristics of the pod propulsors.

19

Han et al. (2000) used a potential-based panel method to solve the flow around the pod configuration including strut and fins and a vortex lattice method to solve the flow around the propeller. The circulation and thickness distributions of the propeller are discredited using a lattice of chordwise and spanwise line vortex and source elements espectively. The pod, strut and their wake surface are discretized with hyperboloidal panels, and normal dipoles and sources having constant strength are distributed on the panels. The Kutta condition is applied to eliminate the pressure jump at the trailing edge of the pod through an iterative process. The mutual interaction between propeller and pod is assumed to be independent of time, which is justified only for mean performance of the propeller and the pod. The predicted performance of the podded propeller overestimated the measurements for moderately loaded condition. Paik et al. (2002) used a similar model to study a contra-rotating podded propeller and got better agreement with measurements for moderately loaded conditions. Kim and Kim (2001) also made similar study for tractor and pusher type podded propellers, but they used only panel method for the computation.

Funeno (2003) described hydrodynamic development of the KHI's podded propulsion system where the geometry of the pod and the strut had been optimized by means of numerical simulation technique based on the commercial Computational Fluid Dynamics (CFD) software STAR-CD. The Reynolds Averaged Navier-Strokes' Equations (RANSE) for incompressible fluid is applied to analyze the viscous flow around the podded propulsor. A steady analysis based on sink-disc method as effects of propeller race is applied to optimize the pod and strut shape in straight course. A quasi-steady analysis method and an unsteady analysis method are applied to analyze the flows around the final pod shape with full geometry of the propeller in straight and oblique flow. The

grid generation is based on the unstructured grid technique. Results of an investigation of unsteady hydrodynamic forces acting on the whole equipment in neutral and oblique rudder angles are given. Based on open water tests and cavitation tests conducted with the final pod shape, computed results are verified.

Gupta (2004) describe to develop and validate a robust method to determine the flow around a podded system, total forces and pod-propeller interaction in various propeller configurations and yaw angles. A Finite Volume Method (FVM) based Euler solver is used to predict the flow around the pod and strut. The flow field around the propellers and forces on the propeller blades are determined using a Vortex Lattice Method (VLM).

Islam (2004) describes the effects of propeller hub taper angle and pod strut geometry configuration on propulsive performance by using surface panel method. The effect of taper angle is determined in terms of thrust coefficient, torque coefficient for different taper angle for both push and pull type podded propellers. But he computes the effects of hub taper angle for $15°$ and $20°$ only. In the present research, the effects of hub taper angle for $5°$, $10°$, $15°$, $20°$ and $25°$ are computed both for conventional propeller and podded propeller, i.e., propeller attached to pod-strut geometry. A computer code for analyzing marine propeller in steady flow using potential based surface panel method has been extended to analyze the complete podded propulsion system.

CHAPTER 3

3. METHODOLOGY

This chapter consists of a brief discussion of the problems that are addressed in the current research work and discuss the methods used to handle these problems.

3.1 Identification of Problems

In practical fields propellers hubs have various kinds of shapes. In fixed pitch conventional screw propellers use of straighter/cylindrical hubs are most evident. As the concept of podded propulsion is introduced, it is very important to maintain a continuity of profile for the whole unit (pod-strut and the propeller), which is very important from a hydrodynamic point of view. In other words, the hub profile shape should be designed in such a way that it matches (maintains continuity) with the main pod body profile. Hence, on a regular basis a tapered hub profile (conical hub) is used in podded propulsors. Due to this introduction of the tapered hub, the flow field around the propeller changes, which results in changing the hydrodynamic characteristics of the propeller as compared to performance of a straight hub propeller.

Some research work have been done on propeller boss cap fins [Ouchi, 1988 and Black et al., 2001] which are fitted to tapered hub cone behind propeller boss. These papers basically addressed the effects of boss cap fins on propeller performance but did not address the effect of taper hub on propeller performance. Numerical prediction of effects of hub taper angle on the hydrodynamic characteristics of a propeller is one of the main tasks of this research work. The hub taper angle for a pusher podded propulsor and a puller podded propulsor are completely opposite. This taper angle changes the inflow

22

angle of attack and the shape of the propeller blade sections, especially around the blade roots (because of the intersection of three surfaces: pressure side and suction side of propeller blade and the root hub). This change in blade sectional geometry and root hub lead to a variation of sectional pressure distribution, hence, propulsive performance. How the taper angle effects the performance is studied numerically in this research work.

In a push type podded propulsion system, the pod-strut body stays forward of the propeller while operating in normal operation (ahead) mode. Due to the presence of the pod-strut body forward of the propeller, the flow fields around the propeller change, which affects the hydrodynamic performance of the propeller. Prediction of the effects of presence of the pod-strut body in push configuration on hydrodynamic characteristics of the propeller is also performed in this research work. In calculating the effect of pod-strut geometry on propeller performance, only the blockage effect (due to the proximity of the pod-strut body), by placing the pod-strut body in front of the propeller. is considered but losses (due to skin friction) associated with the pod-strut body are ignored. Interaction effects between the propeller and pod-strut body are taken into consideration but interaction between the wake and velocity induced by the pod-strut body and the propeller is not taken into consideration.

3.2 Computational Methods

Though many methods are available to solve steady/unsteady lifting problems, probably hyperboloidal/flat-panel source-doublet low/high order panel methods are the most dependable in solving the problems more or less precisely. A well-structured numerical code can increase the versatility of the computations [Liu, 1996]. Predictions of the

23

hydrodynamic characteristics of a screw propeller can be done through a number of numerical methods. These methods can be categorized into the following four families:

- Numerical method based on boundary element theory (Panel methods);

- Numerical method based on unsteady thin wing theory (Lifting line and lifting surface theory);

- Numerical method based on momentum and blade-element theory; and

- Navier-Strokes solvers (Viscous flow theory).

In unsteady lifting line theory, vortices in the flow represent the foil of a wing or propeller blade and it is appropriate only for foils with large aspect ratio. The accuracy of the predictions from this theory for low aspect ratio foils (such as marine propeller blades) is questionable. The lifting surface theory, such as the unsteady QVLM (Quasi Vortex Lattice Method), is a better choice for predicting propeller open water characteristics. However, as for any numerical method, the unsteady QVLM has some disadvantages, such as inability of solving problem for thick leading edge foil section, wing-body combinations and leading edge suction [Liu, 1996].

The panel method is free from the disadvantages stated above. When the leading edge panel descretization is carefully arranged, a panel method is able to take both thickness and wing-body combinations into account, as well as the leading edge suction. The leading edge suction is included inherently in a panel method, though some researchers make comments that the vortices and hence suction are over predicted at the leading edge [Liu, 1996].

24

In this study, a low order potential based surface panel method is used for the hydrodynamic analysis of pod propulsion system because of its robustness with respect to complicated geometry and requires relatively smaller computational effort.

3.3 Surface Panel Method (SPM) or Boundary Element Method (BEM)

There are some mathematical models representing body geometry used for the inviscid analysis of lifting bodies, i.e., wing, hydrofoil, rudder, propeller etc. These models fall into three main categories: lifting-line theory, lifting-surface theory and lifting body theory also known as surface panel method or boundary element method. However, surface panel method [Hess, 1966 and Hess. 1990] uses the exact surface geometry to obtain pressures and velocities and has been remarkably advanced in the fields of aerodynamics and consequently hydrodynamics for the design and analysis of three-dimensional lifting bodies. The method is suitable for analysis of potential flow around three-dimensional body of complicated geometry. The principle lies in representation of the solid body boundaries by a number of small surface elements (panels) with distribution of singularities at the centroid of each panel. In practice, there are many variants of these methods. The most general division distinguishes two groups:

- methods based on velocity potential, i.e., a scalar quantity
- methods based directly on velocity, i. e., a vector quantity

In each of these groups the following further division may apply into:
- low order methods, using constant intensity of hydro-mechanic singularities located on flat panels
- High order methods, using non- linear distributions of hydro- mechanic singularities located on curvilinear panels.

25

Finally, in each method it is possible to employ different types of singularities: vortices, dipoles. sources or combinations of them. It is assumed that the flow is incompressible, irrotational and inviscid. Then an induced velocity potential fulfilling the Laplace equation exists, which may be determined on the basis of the following boundary conditions:

- Kinematics boundary condition on the body surface. postulating zero normal resultant velocity.

- wake surface is infinitely thin, with zero jump of velocity and pressure across it, but with non-zero jump in potential.

In order to ensure numerical simplicity, a low order variant is selected for deriving equation representing the flow around the body by a distribution of sources and dipoles on the body surface and on the wake surface. Discretisation of this equation leads to the system of linear equations with unknown intensities of dipoles. The number of unknowns corresponds to the number of elementary panels representing the body surface, with control points and singularity points located in the centre of each panel. Solution of this system leads to determination of the scalar potential field on the boundary. Then the total flow velocity at any point of interest may be determined by numerical differentiation of the potential in any required direction.

Now determination of the resultant hydrodynamic forces on the lifting/nonlifting body is the matter of simple integration. However, it must be kept in mind that the computed pressure field does not include the effects of water viscosity and it should be corrected accordingly using empirical correction coefficients. Similarly, the viscous drag forces on each panel should be computed using appropriate empirical relations and should be

26

included in the integration of the hydrodynamic forces.

The above outlined principle of the surface panel method must be now applied to an object having a very complicated geometry, with a number of interacting rotating and non-rotating elements. Each of these elements is represented by a number of flat quadrilateral panels.

The geometry of the pod propulsor is assumed to be given as input data. On the other hand, the geometry of the wake surfaces had to be decided when building the panel model. Strictly speaking, the wake surfaces have to coincide with stream surfaces of the resultant flow composed of the inflow and of the induced velocity fields. This would require a very time consuming iteration process to find the ultimate wake geometry. On the basis of experimental evidence and previous experience with propeller analysis methods it is decided to predefine the wake geometry by means of simple semi-empirical relations. This leads to the following principal features of the wake model employed in this method:

- there is no contraction of the wake surfaces. i.e., their span (radius) equals that of the generator lifting foil

- the pitch angle of the wake surfaces located between inflow field angle and the geometric pitch angle of the generator lifting foil and it is determined on the basis of the latter two angles by means of an empirical relation:

- in order to avoid numerical singularities in integration of potential the wake panels crossing the boundary of the propulsor elements are eliminated from computations.

- according to Kutta condition the dipole intensity on the first wake panel near the foil trailing edge is the difference of dipole intensity on both sides of the foil close to the trailing edge .

27

3.3.1 Mathematical Formulation of Surface Panel Method (SPM)

Consider a lifting body (see Fig. 3.1) in inviscid, incompressible, and irrotational flow of an ideal fluid with a uniform velocity V_I, the basic equation for the perturbation velocity potential at an arbitrary field point $p(x, y, z)$, can be obtained from Green's second identity (Breslin and Andessen, 1994) as expressed

$$4\pi E \phi(p) = \int_S \left[\phi \frac{\partial G}{\partial n} - G \frac{\partial \phi}{\partial n} \right] ds \qquad (3.1)$$

Where,
$$E = \begin{cases} 0 & \text{for the point } p \text{ inside } S \\ \dfrac{1}{2} & \text{for the point } p \text{ on } S \\ 1 & \text{for the point } p \text{ outside } S \end{cases}$$

$\phi(p)$ is the potential at the field point, p, G is the Green's function and S is the boundary surface of the fluid volume, i.e., $S = S_B + S_W{}^+ + S_W{}^-$
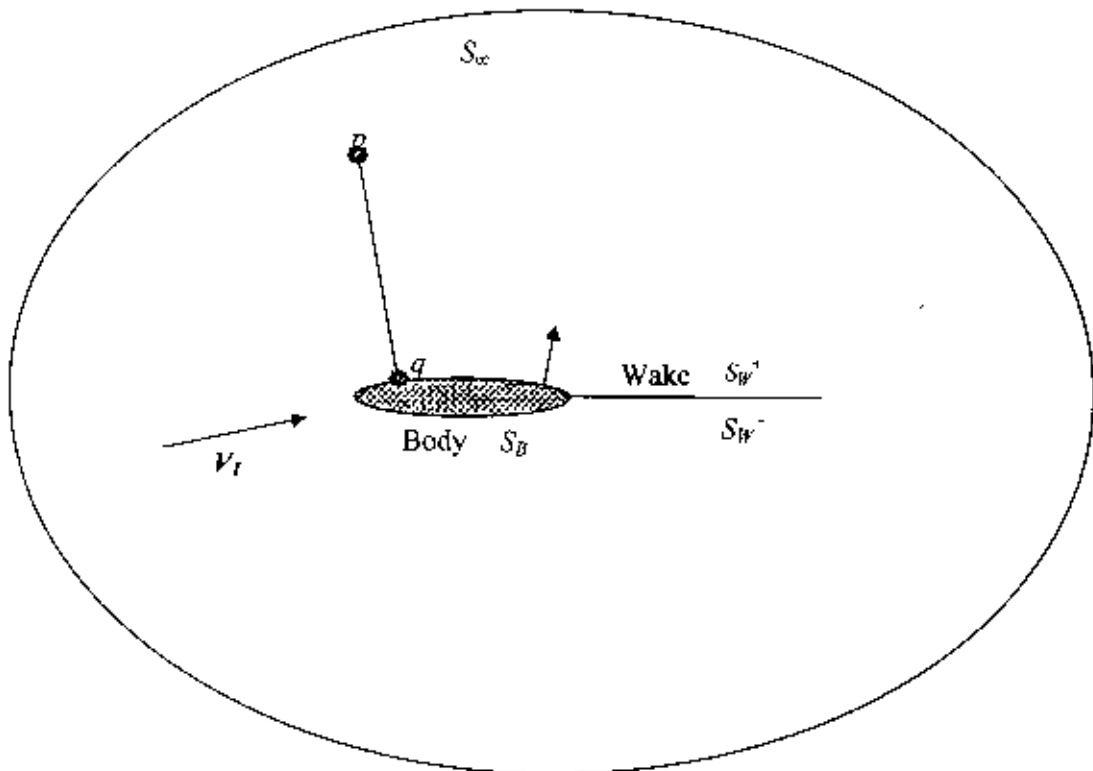
Figure 3.1: Lifting body with its wake

The wake surface can be considered as an infinitely thin domain where the both sides of the surface coincide. So the integral over the wake surfaces S_w^+ (upper side) and S_w^- (lower side) can be collapsed into one single surface S_w and the contribution from the wake can be written as:

$$\phi(p) = \frac{1}{2\pi} \int_{S_w^+ - S_w^-} \left[\phi \frac{\partial G}{\partial n} - G \frac{\partial \phi}{\partial n} \right] ds = \frac{1}{2\pi} \int_{S_w} \left[\phi^+ \frac{\partial G}{\partial n} + \phi^- \frac{\partial G}{\partial n} - G \left(\frac{\partial \phi^+}{\partial n} + \frac{\partial \phi^-}{\partial n} \right) \right] dS \quad (3.2)$$

Since the distance between two points on S_w^+ and S_w^- is infinitely small, the velocity normal to the trailing-vortex sheet is continuous. Then we have $\dfrac{\partial \phi^+}{\partial n} = -\dfrac{\partial \dot\phi^-}{\partial n}$ and the last integral is zero. The first integrand contains the jump in potential across the wake cut $\Delta\phi = \phi^+ - \phi^-$, which is non-zero. Therefore, Equation (3.1) for velocity potential becomes

$$2\pi\phi(p) = \int_{S_B} \left[\phi(q) \frac{\partial}{\partial n_q} \frac{1}{R(p;q)} - \frac{1}{R(p;q)} \frac{\partial}{\partial n_q} \phi(q) \right] dS + \int_{S_w} \Delta\phi(q) \frac{\partial}{\partial n_q} \frac{1}{R(p;q)} dS \ (3.3)$$

where Green's function, G expressed as $G = \dfrac{1}{R(p;q)}$, $R(p;q)$ being the distance between the field point $p(x,y,z)$ and the boundary point $q(\xi,\eta,\zeta)$.

So the velocity potential, ϕ is the superposition of potentials of distributions of strength, $\dfrac{\partial\phi}{\partial n}$ and normal dipoles of strength, ϕ on the surface of the body plus a distribution of dipoles on the wake surface, S_w of strength. $\Delta\phi$. Equation (3.3) is a Fredholm integral equation of second kind for the velocity potential, ϕ and can be solved uniquely. The resulting surface potential distribution can be differentiated to obtain velocities and pressure, which are integrated to yield the total forces and momentum.

29

3.3.2 Discretization of the Singularity Distribution

The Equation (3.3) will lead a linear algebraic equation system for the unknown ϕ_i by discretization as:

$$2\pi\phi_i = \sum_{\substack{j=1 \\ (i\neq j)}}^{N} D_{ij}(\phi_j) + \sum_{j=1}^{N_R} \sum_{i=1}^{N_{lW}} W_{ijl}(\varDelta\phi)_j + \sum_{j=1}^{N} S_{ij}(\frac{\partial\phi}{\partial n})_j, \quad i = 1,2......N \qquad (3.4)$$

where W_{ijl} is the constant dipole distribution, S_{ij} is the constant source distribution and D_{ij} is the influence coefficients on panel j acting on the control point of panel i, defined as

$$D_{ij} = \sum_{k=1}^{K} \left[\int_{S_j} \frac{\partial}{\partial n}\left(\frac{1}{R_{ijk}}\right)dS_j \right]; \quad W_{ijl} = \sum_{k=1}^{K} \left[\int_{S_l} \frac{\partial}{\partial n_l}\left(\frac{1}{R_{ilk}}\right)dS_l \right]; \quad S_{ij} = -\sum_{k=1}^{K} \left[\iint_{S_j}\left(\frac{1}{R_{ijk}}\right)dS_j \right];$$

ϕ_j, $\varDelta\phi_j$ and $(\frac{\partial\phi}{\partial n})_j$ are the strength of dipole and source on panel j, among which $(\frac{\partial\phi}{\partial n})_j$ is predetermined from the boundary condition. N is the total number of panels on the body surface, N_R is the number of the radial panels on the body surface and N_W is the number of wake panels for each radial panels. These influence coefficient D_{ij}, W_{ijl} and S_{ij} will be evaluated by Morino's analytical equation (See Appendix 1) with these results the system of equation can be written in matrix form

$$[D]\{\varPhi\} = [S] + [W][\varDelta\varPhi]$$

where,

$[D]$ = the influence coefficient matrix of dipole induced potential

$[S]$ = the influence coefficient matrix of the source induced potential

$[W]$ = the influence coefficient matrix of the dipole induced potential

$\{\varPhi\}$ = the unknown perturbation potential

30

$[\Delta\Phi]$ = the unknown potential jump at the trailing edge of the blade

The Gauss-Seidel method will be used here for the solution of linear of equations to yield the value of unknown potential.

3.3.3 Kinematic Boundary Condition

The kinematic boundary condition is that the velocity normal to the boundary surface should be zero. Using the inflow velocity $\vec{V}_I$, the boundary condition can be written as

$$\frac{\partial \phi}{\partial n} = -\vec{V}_I \bullet \vec{n}_q \tag{3.5}$$

where, $\vec{n}_q$ is the unit normal vector at a point q on the boundary.

3.3.4 Pressure Kutta Condition

The Kutta condition requires that the velocity at the trailing edge of the lifting body be finite. In the numerical formulation of the problem, the Kutta condition can be implemented by requiring that the pressures at the upper and lower control points at the trailing edge be equal. This can be expressed by

$$\Delta p_j = p_j^U - p_j^L = 0 \qquad for \quad j = 1, N_R \tag{3.6}$$

A direct solution of the resulting system of Equations (3.4) and (3.6) is difficult due to the non-linear characteristic of the Equation (3.6). Therefore an iterative solution algorithm as Kerwin et al. (1987) is employed. At the k-th iteration, the linear system of equation is solved with the values $\Delta\phi_j(k)$ determined from the $(k-1)$-th iteration. The values of $\Delta p_j(k)$ are given by Equation (3.6), with the values of the pressures p_j^U and p_j^L determined as described later. If $\Delta p_j(k)$ is not equal to zero within the desired tolerance

$(\varepsilon = 1E - 5)$. we proceed to iteration with $\Delta\phi_j(k+1)$ determined as follows:

$$[\Delta\phi]^{(k+1)} = [\Delta\phi]^k - [J]^{-1}.[\Delta p]^k \tag{3.7}$$

where $[\Delta p] = [\Delta p_1, \Delta p_2, \ldots\ldots, \Delta p_{N_R}]^T$: $[\Delta\phi] = [\Delta\phi_1, \Delta\phi_2, \ldots\ldots, \Delta\phi_{N_R}]^T$

and $[J]^{-1}$ is the inverse of the Jacobian matrix, the elements of which are defined as:

$$J_{ij} = \frac{\partial(\Delta p_i)}{\partial(\Delta\phi_j)} = \begin{bmatrix} \dfrac{\partial(\Delta p_1)}{\partial(\Delta\phi_1)} & \dfrac{\partial(\Delta p_1)}{\partial(\Delta\phi_2)} & \dfrac{\partial(\Delta p_1)}{\partial(\Delta\phi_3)} & \cdots\cdots\dfrac{\partial(\Delta p_1)}{\partial(\Delta\phi_{N_R})} \\[2mm] \dfrac{\partial(\Delta p_2)}{\partial(\Delta\phi_1)} & \dfrac{\partial(\Delta p_2)}{\partial(\Delta\phi_2)} & \dfrac{\partial(\Delta p_2)}{\partial(\Delta\phi_3)} & \cdots\cdots\dfrac{\partial(\Delta p_2)}{\partial(\Delta\phi_{N_R})} \\[2mm] \dfrac{\partial(\Delta p_3)}{\partial(\Delta\phi_1)} & \dfrac{\partial(\Delta p_3)}{\partial(\Delta\phi_2)} & \dfrac{\partial(\Delta p_3)}{\partial(\Delta\phi_3)} & \cdots\cdots\dfrac{\partial(\Delta p_3)}{\partial(\Delta\phi_{N_R})} \\[2mm] \cdots & \cdots & \cdots & \\ \dfrac{\partial(\Delta p_{N_R})}{\partial(\Delta\phi_1)} & \dfrac{\partial(\Delta p_{N_R})}{\partial(\Delta\phi_2)} & \dfrac{\partial(\Delta p_{N_R})}{\partial(\Delta\phi_3)} & \cdots\cdots\dfrac{\partial(\Delta p_{N_R})}{\partial(\Delta\phi_{N_R})} \end{bmatrix} \tag{3.8}$$

with the values of the partial derivatives approximated numerically as:

$$\frac{\partial(\Delta p_i)}{\partial(\Delta\phi_j)} \approx \frac{\Delta p_i^{(\beta)} - \Delta p_i^{(0)}}{\Delta\phi_j^{(\beta)} - \Delta\phi_j^{(0)}} \tag{3.9}$$

where $\Delta p_i^{(0)}$ corresponds to the initial guess $\Delta\phi_j^{(0)}$ and $\Delta p_i^{(\beta)}$ correspond to $\Delta\phi_j^{(\beta)}$, a perturbation to the initial guess defined as:

$$\Delta\phi_j^{(\beta)} = (1 - \beta)\Delta\phi_j^{(0)}$$

and $\qquad\qquad\qquad\qquad\qquad$ (3.10)

$$\Delta\phi_l^{(\beta)} = \Delta\phi_l^{(0)} \quad for \quad l \neq j$$

where β is very small number which can be 0.01. The initial guess $\Delta\phi_m^{(0)}$ is obtained by Morino-Kutta condition, i.e., the difference of the potentials at the upper and lower control points at the trailing edge.

$$\Delta\phi_m^{(0)} = \phi_m^U - \phi_m^L \tag{3.11}$$

32

3.3.5 Computation of Pressure Distribution

After the computation of the velocity potential on the surface, the velocity and pressure on the surface can be obtained by differentiating the velocity potential over the body surface according to the method proposed by Yangizawa (1984). The distribution of velocity potential is approximated by a quadratic equation passing through the potentials at the centroids of three adjacent panels as (Hoshino, 1989):

$$\phi = aS^2 + bS + c$$

Where S is the surface distance and a, b and c are the coefficients of the quadratic equation. Then the derivatives of the potentials along the tangent directions S_1 and S_2 to panel surface can be expressed as:
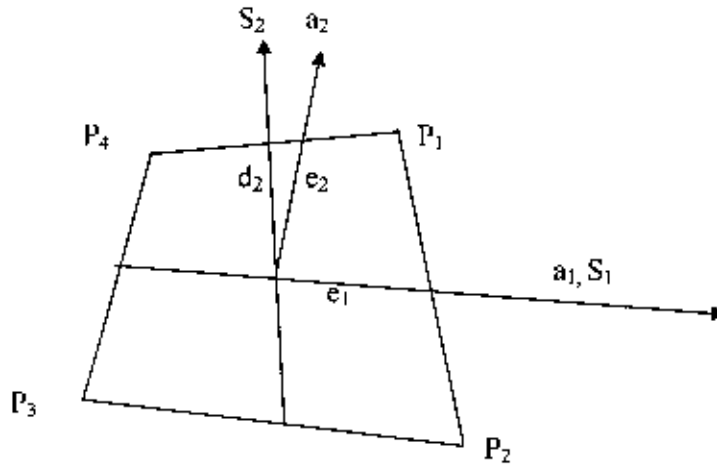
Figure 3.2: Local coordinate system on a panel

$$\frac{\partial \phi}{\partial S_1} = \phi_{S,1} = 2a_1 S_1 + b_1$$

$$\frac{\partial \phi}{\partial S_2} = \phi_{S,2} = 2a_2 S_2 + b_2$$

Next, we take the a_1 axis in the direction of S_1 and the a_2 axis in the direction perpendicular to S_1 in the plane composed of S_1 and S_2 as shown in Figure 3.2.

Denoting the unit vectors in the directions of a_1, a_2 and S_2 axes by e_1, e_2 and d_2 respectively, the derivatives of the potential along a_1 and a_2 axes can be expressed as

$$\phi_{a,1} = \frac{\partial \phi}{\partial a_1} = \phi_{S,1}$$

$$\phi_{a,2} = \frac{\partial \phi}{\partial a_2} = \frac{\phi_{S,2} - (\vec{d}_2 \cdot \vec{e}_1)\phi_{S,1}}{(\vec{d}_2 \cdot \vec{e}_2)}$$

Then the perturbation velocity tangent to the body surfaces can be obtained by:

$$\vec{v}_t = \phi_{a,1} \, \vec{e}_1 + \phi_{a,2} \, \vec{e}_2$$

Adding the tangential components of the relative inflow velocity, V_I, we obtain the total tangential velocity to the body surface as

$$\vec{V}_t = \vec{V}_I - (\vec{V}_I \cdot \vec{n})\vec{n} + \vec{v}_t$$

$$= \left[(\vec{V}_I \cdot \vec{e}_1) + \phi_{a,1} \right]\vec{e}_1 + \left[(\vec{V}_I \cdot \vec{e}_2) + \phi_{a,2} \right]\vec{e}_2$$

where, $\vec{n} = \vec{e}_1 \times \vec{e}_2$

The pressure on the body surface can be obtained by using Bernoulli's equation

$$p = p_\infty + \frac{1}{2} \rho \left[\left|\vec{V}_I\right|^2 - \left|\vec{V}_t\right|^2 \right]$$

where p_∞ = Static pressure at infinity

ρ = Density of water

Finally the pressure on propeller blade is expressed in terms of non-dimensional pressure coefficient C_p defined as:

$$C_p = \frac{p - p_\infty}{\frac{1}{2}\rho V_I^2} \tag{3.12}$$

where, $V_I = \sqrt{V_A^2 + (2\pi n r)^2}$ and V_A = Velocity of advance.

34

and the pressure on the pod body is expressed in terms of non-dimensional pressure coefficient C_p defined as:

$$C_p = \frac{p - p_\infty}{\frac{1}{2}\rho V_t^2} \qquad (3.13)$$

where, $V_t = V_\infty$.

V_∞ = free stream velocity

3.4 Discretization of the Propeller

The propeller blade. hub and wake surfaces are divided into a number of small quadrilateral hyperboloidal panels. The cosine spacing which concentrates the panel strips at the hub. tip, leading and trailing edges can be used for both the radial and chord wise distribution of panel.

In the radial distribution

$$r_B = \frac{1}{2}(R + r_h) - \frac{1}{2}(R - r_h)\cos\alpha_m \qquad (3.14)$$

In the chord wise distribution

$$C_B = S(r) + \frac{C(r)}{2}\left(1 - \cos\left(\frac{\pi n}{N_C}\right)\right); \quad n = 0, 1, 2, ..., N_C \qquad (3.15)$$

where, $\alpha_m = \begin{cases} 0 & for \quad m = 1 \\ \dfrac{(2m-1)\pi}{2(N_R + 1)} & for \quad m = 2, 3, ..., N_R + 1 \end{cases}$

N_C = Number of chord wise panels

N_R = Number of radial panels

R = Propeller Radius

r_h = Rub Radius

35

$C(r)$ = Chord length of the blade

$S(r)$ = distance from the generator line to leading edge

The propeller hub is divided into three portions: such as. downstream portion, blade portion and upstream portion. The downstream and upstream portions are easy to paneling. In these sections, the hub is treated as a cylinder or ellipsoid. The blade portion is divided into some strips equally spaced in circumferential angle between the roots of blades. These generate the panels with helical pattern on the hub. In the intersection portion the grid consists of only one strip of panels, which match the corresponding panels on the blade. The actual wake behind the propeller is very complicated to analyze. So we look for a mathematical model to simulate the wake behind the propeller. Here, a linear wake model is employed without considering the contraction of slipstream.

3.5 Forces acting on the propeller

The total forces and torque acting on the propeller can be obtained by two components of pressure and friction over the blade. Then the total forces and torque are expressed as:

$$T = K\sum_{i=1}^{N} p(P_i)n_{xi} \cdot \Delta S_i - T_F \tag{3.16}$$

$$Q = K\sum_{i=1}^{N} p(P_i)(n_{yi} \cdot z_i - n_{zi} \cdot y_i)\Delta S_i + Q_F \tag{3.17}$$

where,

ΔS_i : area of panel

(x_i, y_i, z_i) : coordinate of P_i

(n_{xi}, n_{yi}, n_{zi}) : components of outward normal vector, n_i

K : number of propeller blade.

36

The skin friction coefficient, C_f due to viscosity can be obtained by Prandtl-Schlicting formula as:

$$C_f(j) = \left(1 + \frac{t_{max}(j)}{C(j)}\right) \frac{0.455}{(log_{10} Re)^{2.58}} \tag{3.18}$$

where, Re is the Reynolds number and expressed as:

$$Re = \frac{V_i(j).C_j}{\nu}$$

and $\dfrac{t_{max}(j)}{C(j)}$: maximum thickness ratio at each blade section,

$\quad C(j)$: expanded chord length,

$\quad V_i(j)$: local velocity

Then the viscous component of thrust, T_F and torque, Q_F of the propeller can be expressed as:

$$T_F = \frac{1}{2}\rho\, K \sum_{r=1}^{N} C_f(P_r) V_{txi} \left|\vec{V}_{tt}\right| \Delta S_r \tag{3.19}$$

$$Q_F = \frac{1}{2}\rho\, K \sum_{r=1}^{N} C_f(P_j)(V_{txi} \cdot y_r - V_{tyi} \cdot z_r) \left|\vec{V}_{tt}\right| \Delta S_r \tag{3.20}$$

Finally, the non-dimensional characteristics of propeller performance is

Advance coefficient, $\quad J = \dfrac{V_A}{n\,D}$ \hfill (3.21)

Thrust coefficient, $\quad K_T = \dfrac{T}{\rho\, n^2 D^4}$ \hfill (3.22)

Torque coefficient, $\quad K_Q = \dfrac{Q}{\rho\, n^2 D^5}$ \hfill (3.23)

Propeller efficiency, $\quad \eta = \dfrac{J}{2\pi} \cdot \dfrac{K_T}{K_Q}$ \hfill (3.24)

37

Where,

D = Overall diameter of the propeller

n = Rotational speed of the propeller in rev/sec

ρ = fluid density

T = propeller axial thrust force

Q = propeller shaft torque

V_r = mean inflow velocity

$$\% \text{ of } K_T = \frac{\left| K_T \; PPS \; (\text{Hub taper angle}) - K_T \; Prop. \; (\text{Hub taper angle}) \right|}{K_T \; Prop. \; (\text{Hub taper angle})} \times 100 \qquad (3.25)$$

$$\% \text{ of } K_Q = \frac{\left| K_Q \; PPS \; (\text{Hub taper angle}) - K_Q \; Prop. \; (\text{Hub taper angle}) \right|}{K_Q \; Prop. \; (\text{Hub taper angle})} \times 100 \qquad (3.26)$$

$$\% \text{ of } \eta = \frac{\left| \eta \; PPS \; (\text{Hub taper angle}) - \eta \; Prop. \; (\text{Hub taper angle}) \right|}{\eta \; Prop. \; (\text{Hub taper angle})} \times 100 \qquad (3.27)$$

3.6 Hub Taper Angle

To maintain continuity of the profile and smooth flow over the body of a podded propeller, the hub of the propeller is usually tapered. In other words, a conical hub is use for a podded propeller instead of a straight/cylindrical hub. Figure 3.3 shows how a tapered hub ensures the continuity of the pod body profile.

The hub taper angle is usually measured at the blade root section about the geometric center of the propeller. The sign convention that is used in the modeling of the tapered hub is shown in Figure 3.3. A positive hub taper angle is used for push podded propeller configuration and it reduces the diameter of the straight hub in the downstream direction. In other words, for pusher propeller configuration, the leading edge area is smaller and

the trailing edge area is larger compared to that of a straight hub propeller. In contrast negative hub taper angle reduces the hub diameter in the upstream direction and is used in puller propeller configuration. In other words, for puller propeller configuration, the leading edge area is smaller and the trailing edge area is larger compared to that of a straight hub propeller.
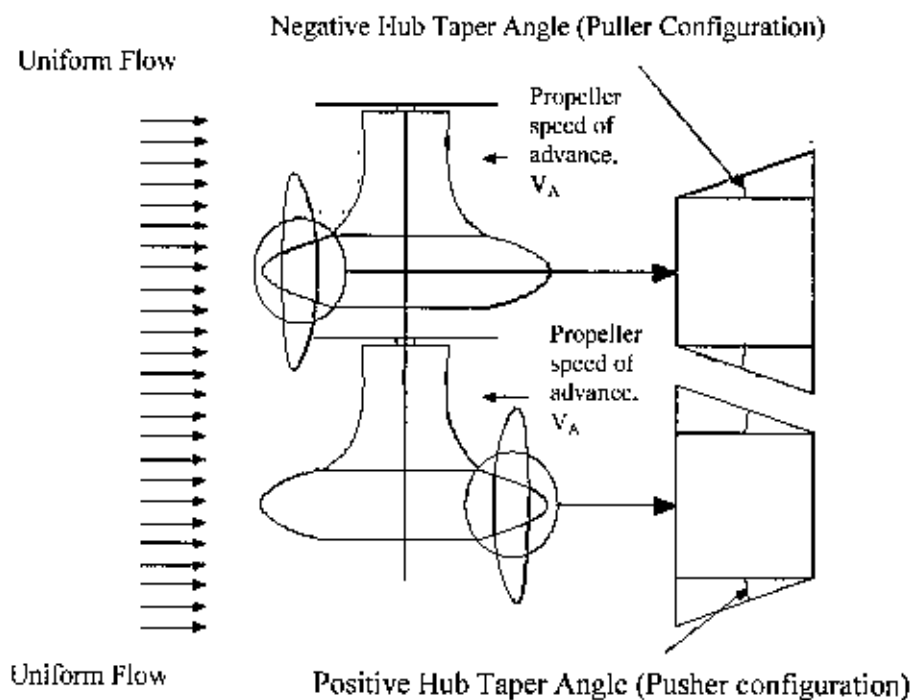
Figure 3.3: Hub taper angle.

CHAPTER 4

4. RESULTS AND DISCUSSION

In this chapter firstly, the potential based Surface Panel Method (SPM) is used to compute the pressure distribution in terms of pressure coefficient, C_p on the isolated axisymmetric pod and underwater bodies, strut, and then pod with strut. The predicted results are compared with published experimental/numerical results. Secondly, the geometry of the marine propeller is described and the hydrodynamic characteristic of the conventional propeller (CP) and DTRC4119 propellers are computed with surface panel method. The computed results are also compared with experimental measurements. Thirdly, a comparative study is done for open water hydrodynamic characteristic of the propellers with hub taper angle of $0°$, $5°$, $10°$, $15°$, $20°$ and $25°$ in terms of thrust coefficient, K_T, and torque coefficient, K_Q, propulsive efficiency, η for a wide range of advance coefficient, J. Finally, effects of pod-strut geometry on propeller performance are studied by analyzing the hydrodynamic characteristics of the complete pod propulsion system, PPS (Propeller + Pod + Strut) when two pod-strut geometries are attached to the propellers in pusher configurations.

4.1.(a) Axisymmetric Pod

The flow around the pod is assumed to be incompressible, inviscid and irrotational. The geometry of the axi-symmetric pod (Pod A) is given in Appendix 2. The panel size of the Pod A is 29×30. The 3-D grid of the axi-symmetric Pod A is made and the influence coefficients are calculated based on all the panel control points. However, only one strip along the longitudinal direction is shown, and it is assumed that the results on the other

strips would be the same due to axi-symmetry of the pod geometry. The inflow velocity of the pod used here is $u = 1, v = 0, w = 0$. The computed pressure coefficient, C_p on the Pod A are determined and compared with results predicted by Gupta (2004) as shown in Figure 4.2
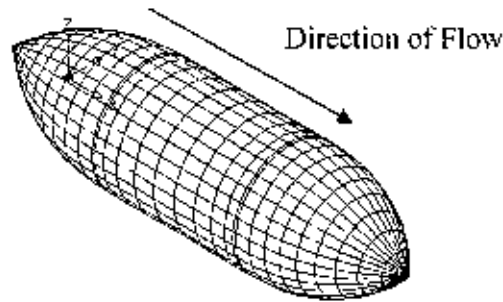
Figure 4.1: Isometric view of Pod A.
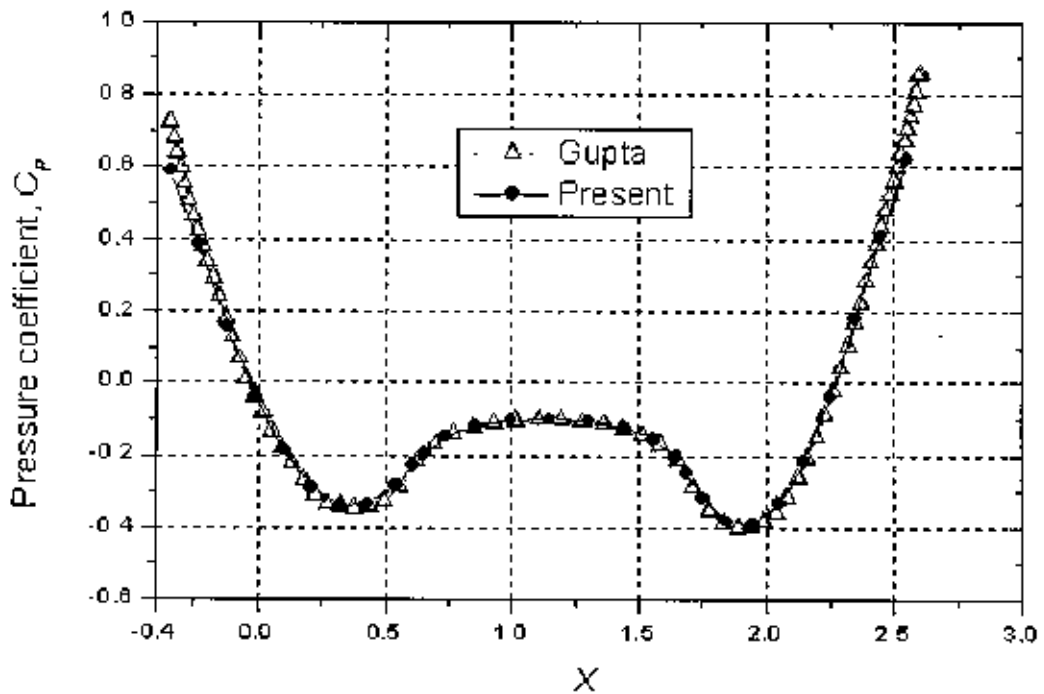
Figure 4.2: Comparison of predicted pressure distribution around axi-symmetric Pod (Pod A) with that computed by Gupta (2004).

Figure 4.2 shows that the predicted results are in a good agreement with results computed by Gupta (2004).

4.1. (b) Axi-symmetric under-water body

The standard hull models of submarine DARPA2 (Defense Advanced Research Projects Agency) geometry is used here. The body is three dimensional which is axisymmetric and its geometry is given in Appendix 2. The panel size of the submerged body is 44×44.
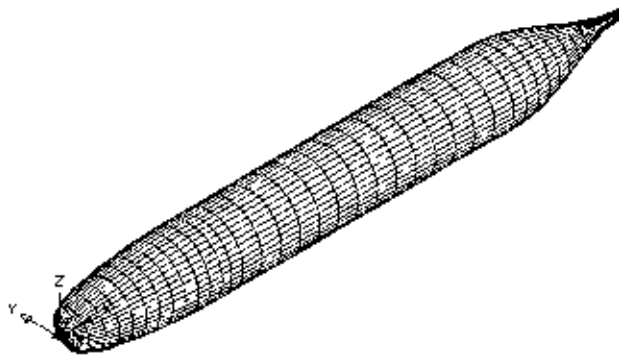
Figure 4.3: Isometric view of submerged under water body.
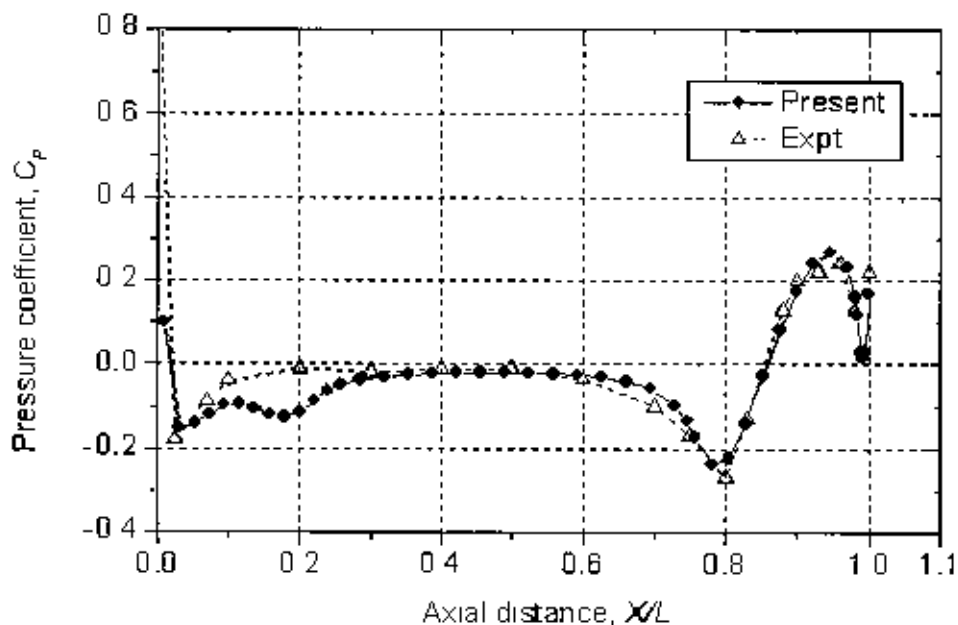
Figure 4.4: Comparison of predicted pressure distribution around DARPA2 submarine

hull with experimental measurements [Sohaib et al., 2006].

42

The inflow velocity used here is $u = 1, v = 0, w = 0$. The pressure coefficient, C_p on the body are determined and compared with experimental results [Sohaib et al., 2006] as shown in Figure 4.4.

From Figure 4.4, it is seen that the predicted results are in a good agreement with experimental results.

4.2. Strut

The strut as shown in Figure 4.5 is formed with NACA0012 wing section and its section data is given in Appendix 2. The panel size of the strut is 34×34. The inflow velocity used here is $u = 1, v = 0, w = 0$. The pressure coefficient, C_p on the strut are determined and compared with experimental results, which is shown in Figure 4.6.
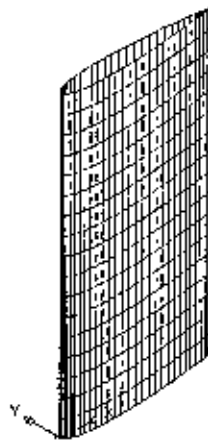
Figure 4.5: Isometric view of strut.
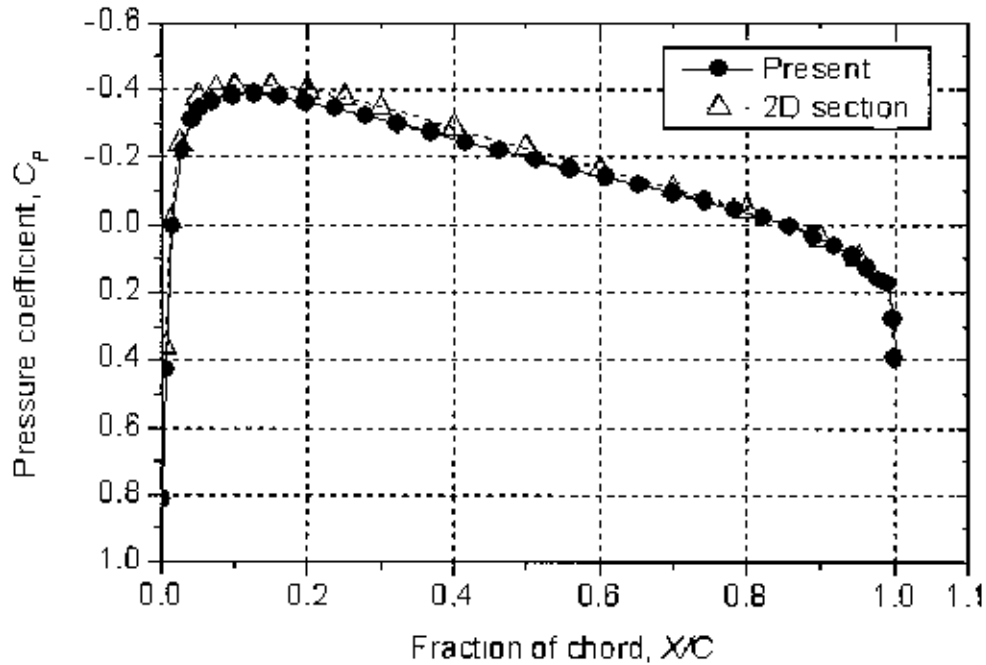
Figure 4.6: Comparison of pressure coefficient around strut (NACA 0012 section) at mid

span with 2D section results [Abbott and Doenhoff, 1959]

From Figure 4.6, it is seen that the predicted results are in a good agreement with 2D

section results.

4.3. Pod with strut

The flow around the pod with strut is assumed to be incompressible, inviscid and

irrotational. Here the body is a three dimensional pod with strut. The geometry of the pod

(Pod B) is given in Appendix 2. The strut is a NACA066 section, with leading edge at the

location $X = -0.6$ on Pod B, and trailing edge at $X = +0.6$, whose geometry are given in

Appendix 2. The panel size of the Pod B is 29×28 and the strut is 11×11. The whole 3-D

grid of the Pod B and strut is made as shown in Figure 4.7 and the influence coefficients

are calculated based on all the panel control points. The inflow velocity of the pod

44

is $u = 1, v = 0, w = 0$. The pressure coefficient, C_p on the Pod B in presence of strut is computed and compared with results predicted by Gupta (2004) as shown in Figure 4.8.
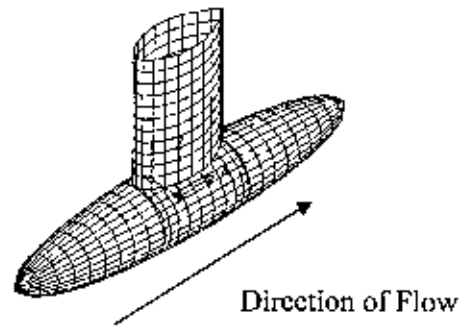
Figure 4.7: Isometric view of Pod B with strut.
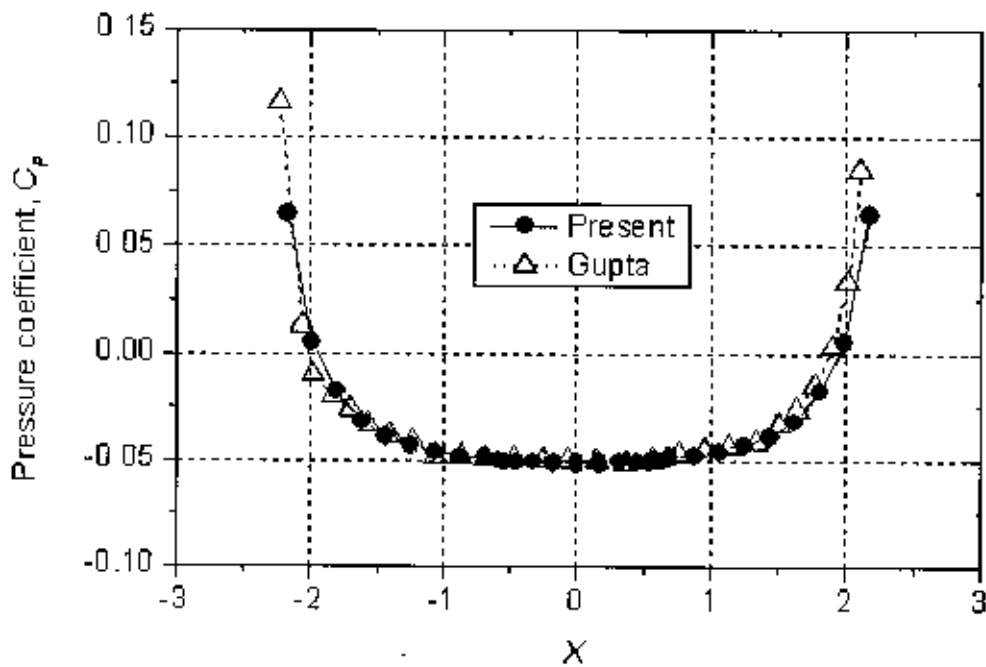
Figure 4.8: Comparison of predicted pressure distribution around Pod (Pod B) with strut with that computed by Gupta (2004).

From Figure 4.8, it is seen that the predicted pressure distribution by the present method is very much close to Gupta (2004).

4.4. Marine Propeller

A propeller is the most common propulsor on ships, imparting momentum to a fluid which causes a force to act on the ship.The ideal efficiency of any size propeller is that of an actuator disc in an ideal fluid. An actual marine propeller is made up of sections of helicoidal surfaces which act together 'screwing' through the water (hence the common reference to marine propellers as "screws"). Three, four, or five blades are most common in marine propellers, although designs which are intended to operate at reduced noise will have more blades. The blades are attached to a boss (hub), which should be as small as the needs of strength allow with fixed-pitch propellers the blades and boss are usually a single casting.

A propeller that turns clockwise to produce forward thrust, when viewed from aft, is called right-handed. One that turns anticlockwise is said to be left-handed. The blade outline is defined either by a projection on a plane normal to the propeller shaft (projected outline) or by setting the circumferential chord across the blade at a given radius against radius (developed outline). The outline is usually symmetrical about a given radial line termed the median. If the median is curved back relative to the direction of rotation the propeller is said to have skew back. The skew is expressed in terms of circumferential displacement at the blade tips. If the blade face in profile is not normal to the axis it is termed raked, expressed as a percentage of total diameter.

Each blade's pitch and thickness varies with radius, early blades had a flat face and an arced back (sometimes called a circular back as the arc was part of a circle), modern propeller blades have aerofoil sections. The camber line is the line through the mid-thickness of a single blade. The camber is the maximum difference between the camber

46

line and the chord joining the trailing and leading edges. The camber is expressed as a percentage of the chord. The radius of maximum thickness is usually forward of the mid-chord point with the blades thinning to a minimum at the tips. The thickness is set by the demands of strength and the ratio of thickness to total diameter is called blade thickness fraction. The ratio of pitch to diameter is called pitch ratio. Blade area is given as a ratio of the total area of the propeller disc, either as developed blade area ratio or projected blade area ratio.

4.4.1 Geometry of the Propeller

Propeller blade geometry can be roughly divided into two parts; the blade outline, which is governed by chord, skew and rake, and the sections, which are governed by pitch, camber and thickness. The coordinate systems and the propeller geometrical notation are shown in Figure 4.9. A propeller-fixed Cartesian coordinate system O-xyz is first defined with origin fixed at the center of the propeller, the x- axis has been taken to coincide with the propeller axis and its direction is positive downstream. The y - axis is at any angular orientation relative to the key blade. The z - axis completes the right-handed system. A cylindrical coordinate system is defined as follows:

$$x = x$$

$$r = \sqrt{y^2 + z^2} \tag{4.1}$$

$$\theta = \tan^{-1}\frac{z}{y}$$

The radial distributions of skew, $\theta_m(r)$, and the rake, $x_m(r)$, define the mid-chord line of the blade as illustrated in Figure 4.10. The leading and trailing edges of the blade are

47

constructed passing a helix of pitch angle, $\phi(r)$ through the mid-chord line can be expressed as:

$$x_{l,t}(r) = x_m(r) \mp \frac{c(r)}{2} \sin \phi(r)$$

$$\theta_{l,t}(r) = \theta_m(r) \mp \frac{c(r)}{2} \cos \phi(r) \qquad\qquad (4.2)$$

$$y_{l,t}(r) = r \cos \theta_{l,t}(r)$$

$$z_{l,t}(r) = r \sin \theta_{l,t}(r)$$

Where $c(r)$ is the chord length a radius r, and the subscripts l and t denote the leading and trailing edges, respectively.
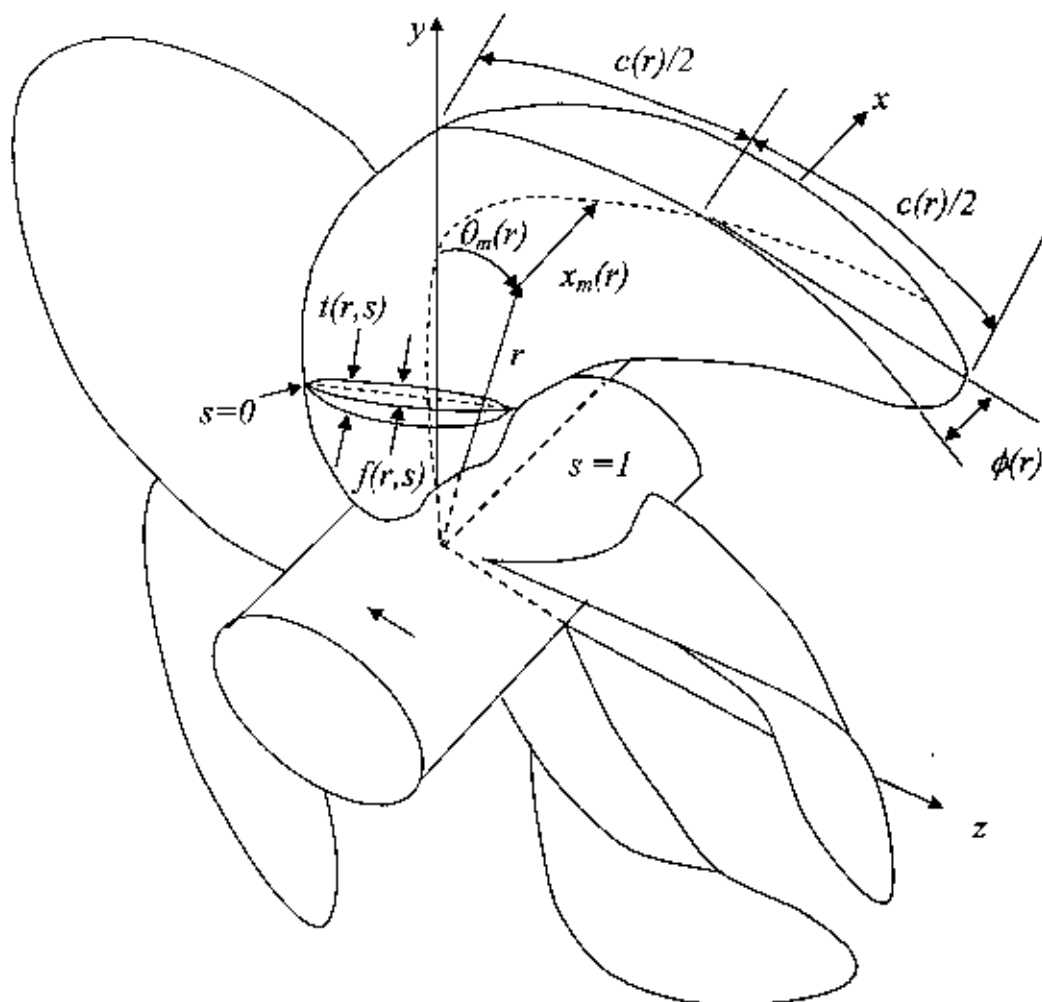
Figure 4.9: Coordinate system and schematic diagram of propeller

48
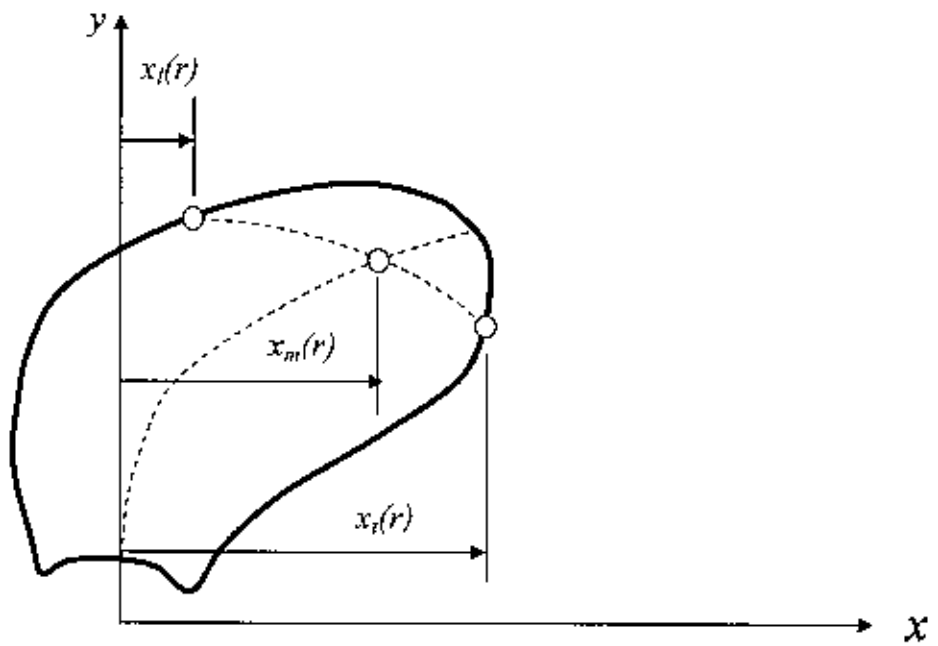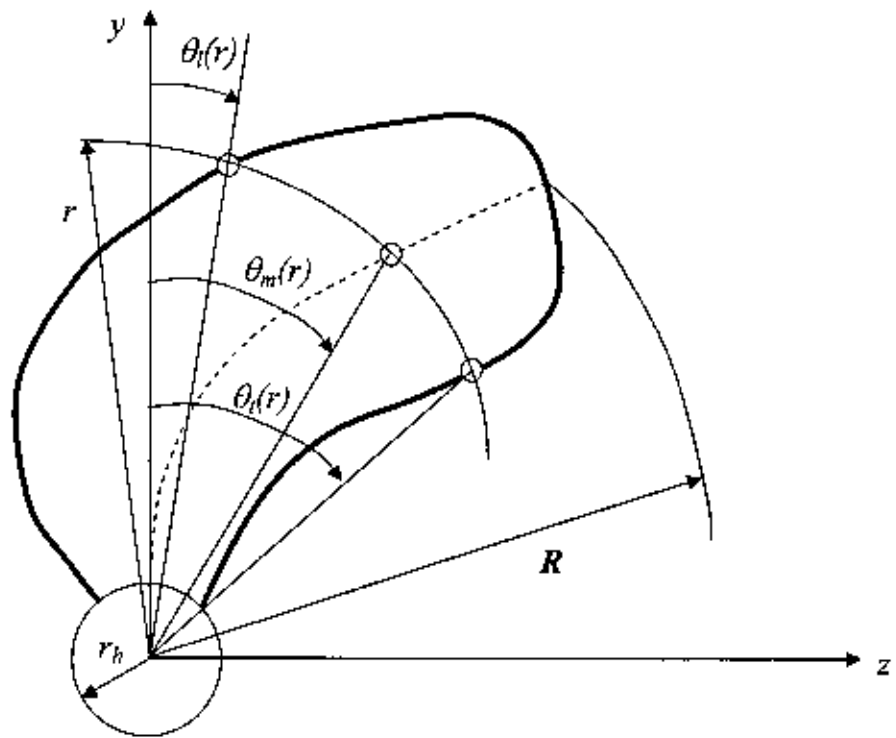
Figure 4.10: Radial distribution of skew and rake
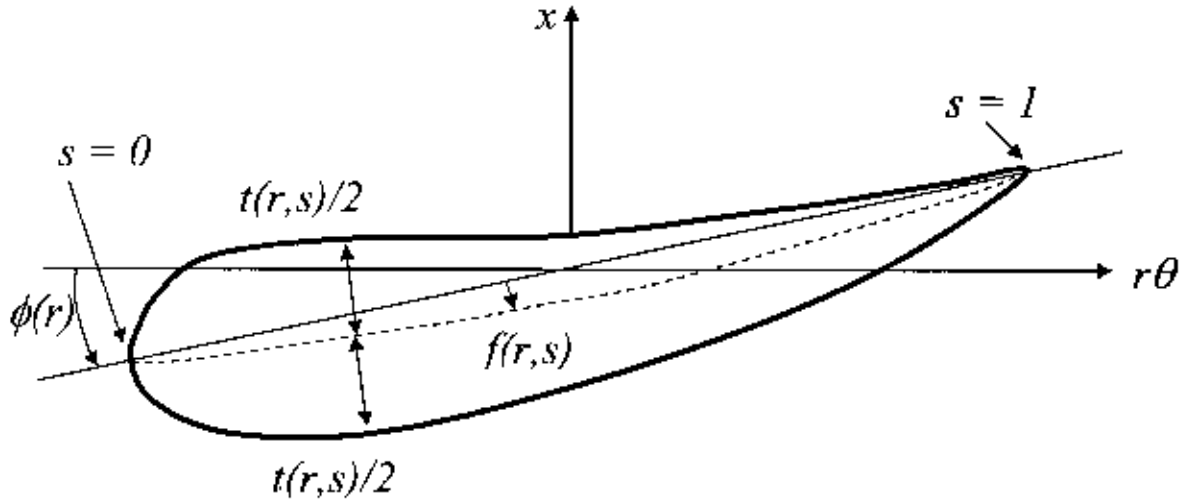
Figure 4.11: Construction of blade section from mean camber line and thickness form.

The camber $f(r,s)$ is measured on the cylindrical surface of radius r normal to the nose-tail helix, where s is a non-dimensional chord-wise coordinate, which is 0 at the leading edge and 1 at the trailing edge.

Finally, the thickness $t(r,s)$ is added symmetrically to the camber line on the cylinder in the normal direction to the mean camber surface as shown in Figure 4.11

$$x_c(r,s) = x_m(r) + c(r)\left(s - \frac{1}{2}\right)\sin\phi(r) - f(r,s)\cos\phi(r)$$

$$\theta_c(r,s) = \theta_m(r) + c(r)\left(s - \frac{1}{2}\right)\frac{\cos\phi(r)}{r} + f(r,s)\frac{\sin\phi(r)}{r} \qquad (4.3)$$

$$y_c(r,s) = r\cos\theta_c(r,s)$$

$$z_c(r,s) = r\sin\theta_c(r,s)$$

The maximum values of $f(r,s)$ and $t(r,s)$ at radius r denoted as the maximum camber, $f_{max}(r)$ and the maximum thickness, $t_{max}(r)$ respectively

50

4.4.2(a) Validation of Predicted Results for SRI Conventional Propeller (CP)

In order to evaluate the accuracy and applicability of the present method, at first comparative study is made for *Ship Research Institute* (SRI) propeller model, which is a conventional propeller designed for a training ship *"Seiun-maru"*. The principal particulars of this propeller are shown in Table 4.1. The panel arrangement of this propeller with linear wake model is shown in Figure 4.12. The chord-wise pressure distributions of conventional propeller are shown in Figures 4.13-4.15 and the results for design advance coefficient, $J = 0.66$ at $r/R = 0.83$ are compared with the experimental values [Karim et al., 2006] at $r/R = 0.8$ as shown in Figure 4.16. The pressures of the back side near the trailing edge are less than the experimental values; however, those on the face side are very much closer to the experimental values. The open water hydrodynamic characteristics of the conventional propeller are compared with experimental values in Figure 4.16. From this figure, it is clear that the predicted values of thrust and torque coefficients are higher than the experimental values but very much closer.

Table 4.1: Pricncipal Particulars of Conventional Propeller (CP)

Type of Propeller	CP
Diameter of propeller (mm)	300
Number of blade	5
Skew angle (deg.)	10.5
Rake angle	6.0
Blade thickness ratio	0.0442
Boss ratio	0.1972
Pitch ratio	0.95 (constant)
Expanded blade area ratio	0.65
Blade section	MAU
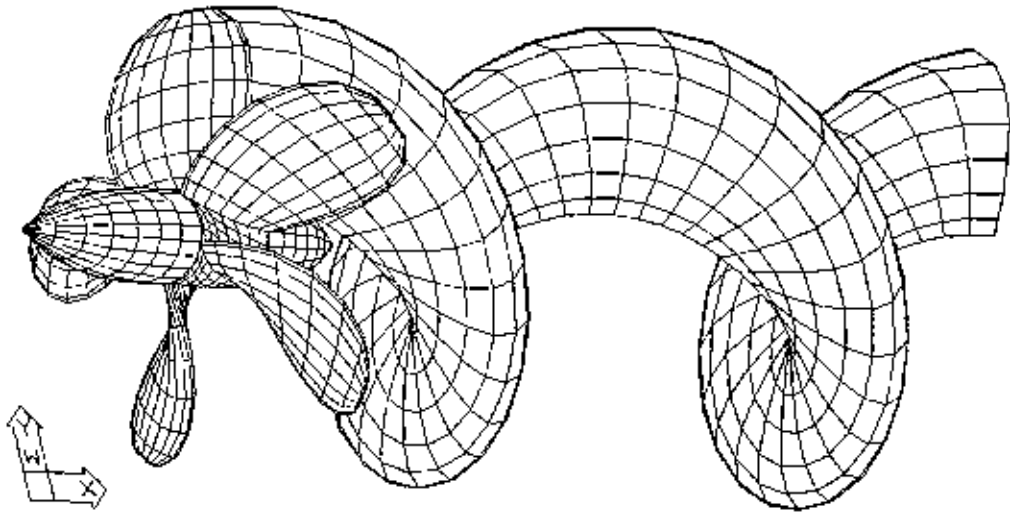
Figure 4.12: Panel arrangement of conventional propeller (9c x 8s) and its wake.
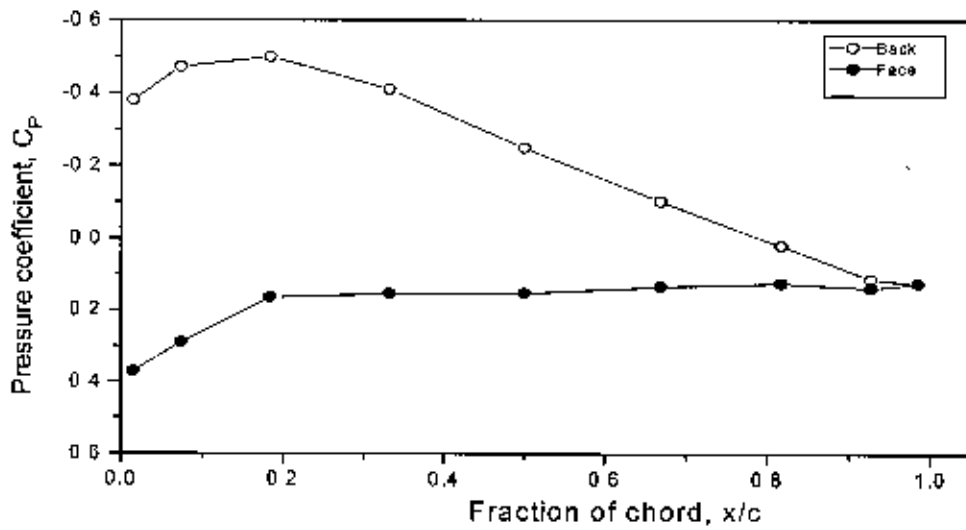
Figure 4.13: Chord-wise pressure distributions of conventional propeller for $J = 0.66$

at $r/R = 0.343$
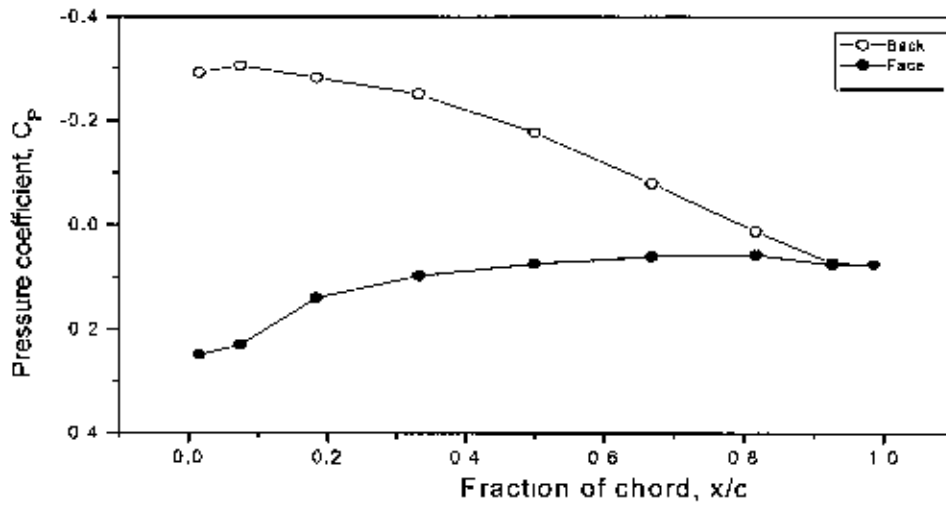
Figure 4.14: Chord-wise pressure distributions of conventional propeller for $J = 0.66$ at $r/R = 0.64$
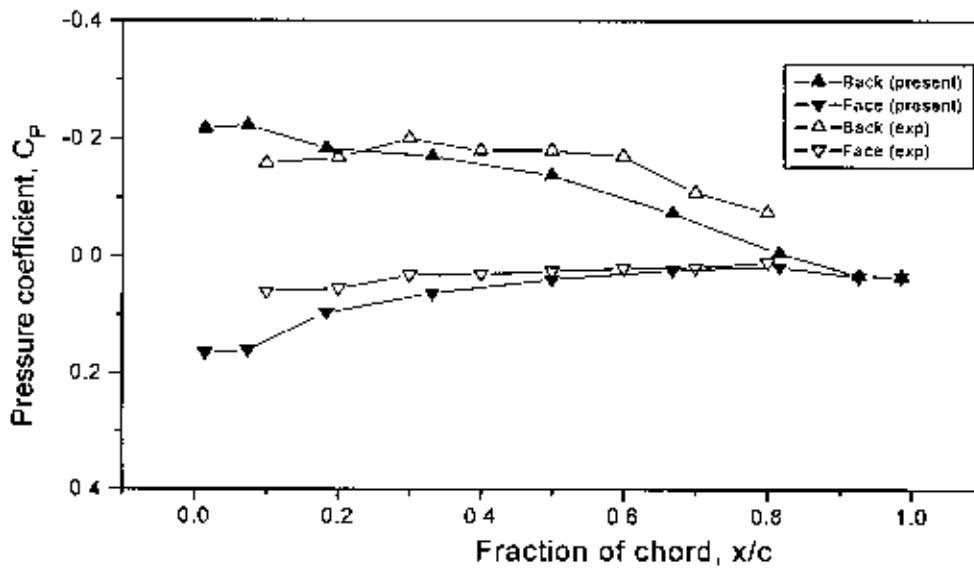
Figure 4.15: Chord-wise pressure distributions of conventional propeller for $J = 0.66$ at $r/R = 0.83$

53
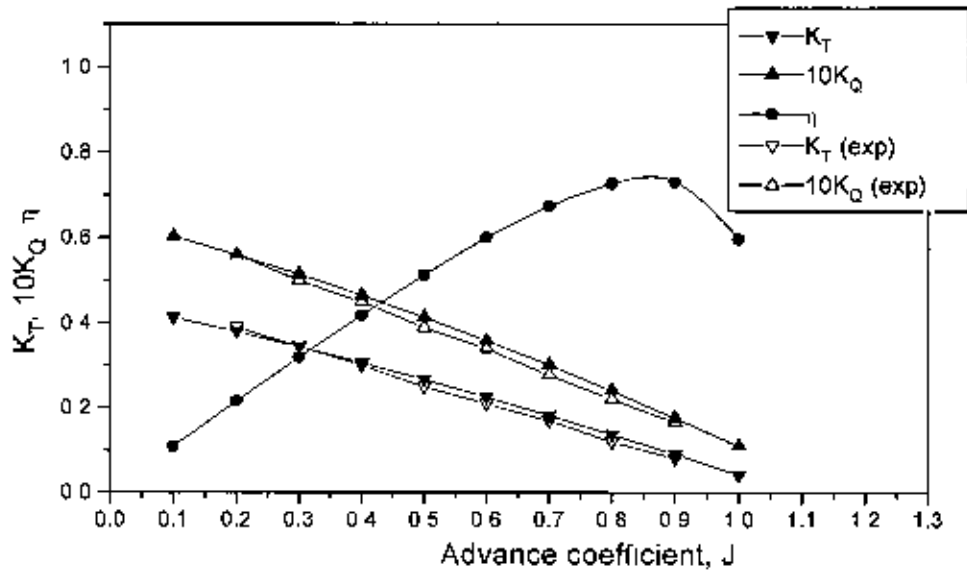
Figure 4.16: Comparison of open water hydrodynamic characteristics of conventional propeller with experimental values.

4.4.2(b) Validation of Predicted Results for DTRC4119 Propeller

For next comparative study, David Taylor Research Center (DTRC) propeller model DTRC4119 is chosen. In this propeller, NACA66 (DTMB modified) thickness form is used combining with $a = 0.8$ meanline. The principal particulars of the propeller is given in Table 4.2 and its panel arrangements are shown in Figure 4.17 with 9 chordwide and 8 spanwise. The chord-wise pressure distributions of the propeller are shown in Figures 4.18-4.20 at designed advance coefficient and compared with the experimental values [Karim et al., 2006]. In each case, the computed results show good agreement with the experimental results except a little discrepancy at $r/R = 0.34$, i.e., near the boss. The open water hydrodynamic characteristics of DTRC4119 propeller are compared with experimental values in Figure 4.21

54

Table 4.2: Principal Particulars of DTRC4119 Propeller

Diameter of propeller (mm)	305
Rotation	Right hand
Number of blade	3
Skew angle (deg.)	0
Rake angle	0
Boss ratio	0.2
Design Advance Coefficient, J	0.833
Section thickness form	NACA66 (DTMB Modified)
Section Meanline	NACA, a = 0.8
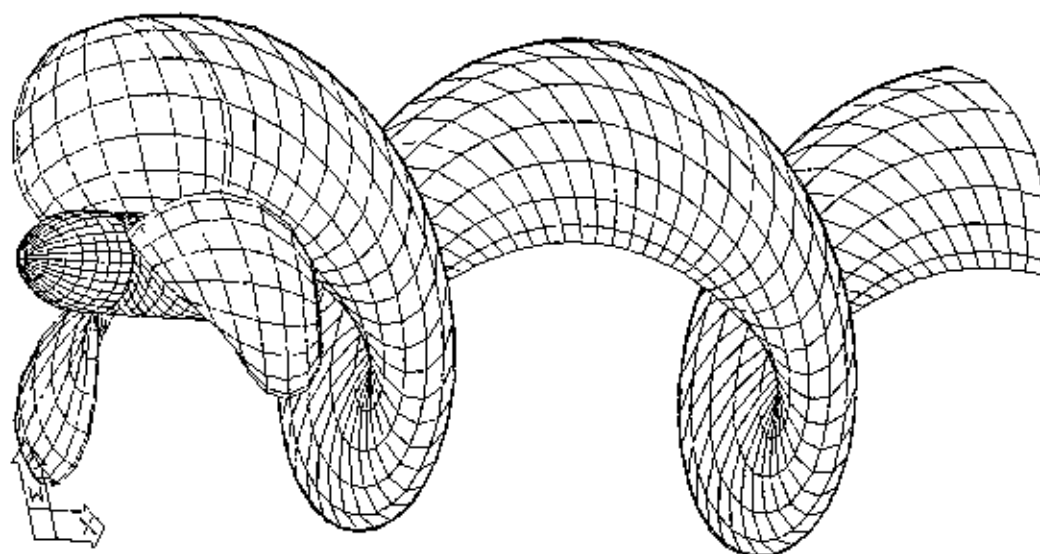
Figure 4.17: Panel arrangement of DTRC4119 propeller (9c x 8s) with its wake.

In this figure, some values of thrust coefficients coincide with the experimental values within the range of advance coefficients, $J = 0.7$-1, but those become larger at higher

values of J and less at lower values of J. The values of torque coefficients become less at lower values of J, make a pivotal point near the design advance coefficient, i.e., $J = 0.833$ and then become higher than the experimental values.
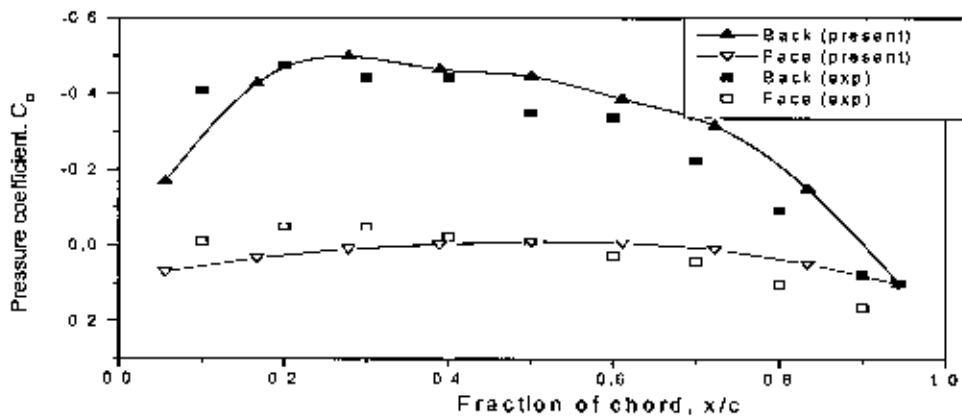
Figure 4.18: Chord-wise pressure distributions of DTRC4119 propeller for $J = 0.833$ at
$r/R=0.34$
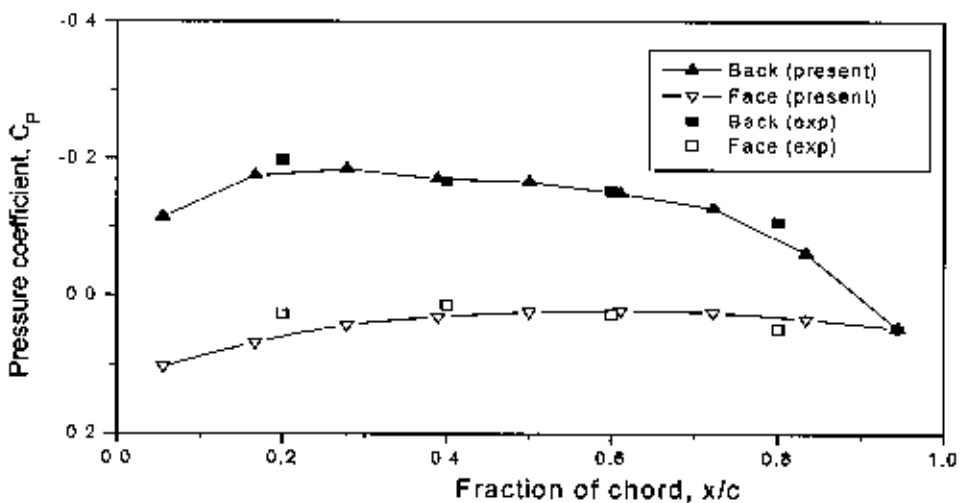
Figure 4.19: Chord-wise pressure distributions of DTRC4119 propeller for $J = 0.833$ at
$r/R=0.73$

56
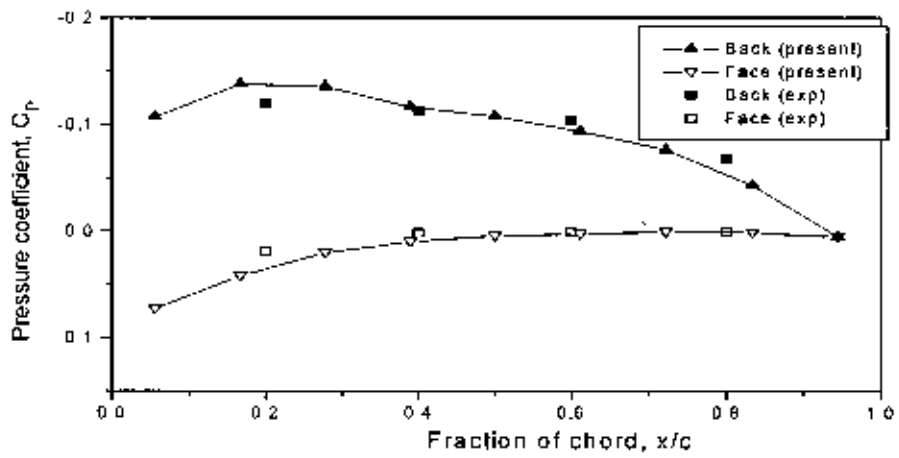
Figure 4.20: Chord-wise pressure distributions of DTRC4119 propeller for $J = 0.833$ at $r/R=0.92$
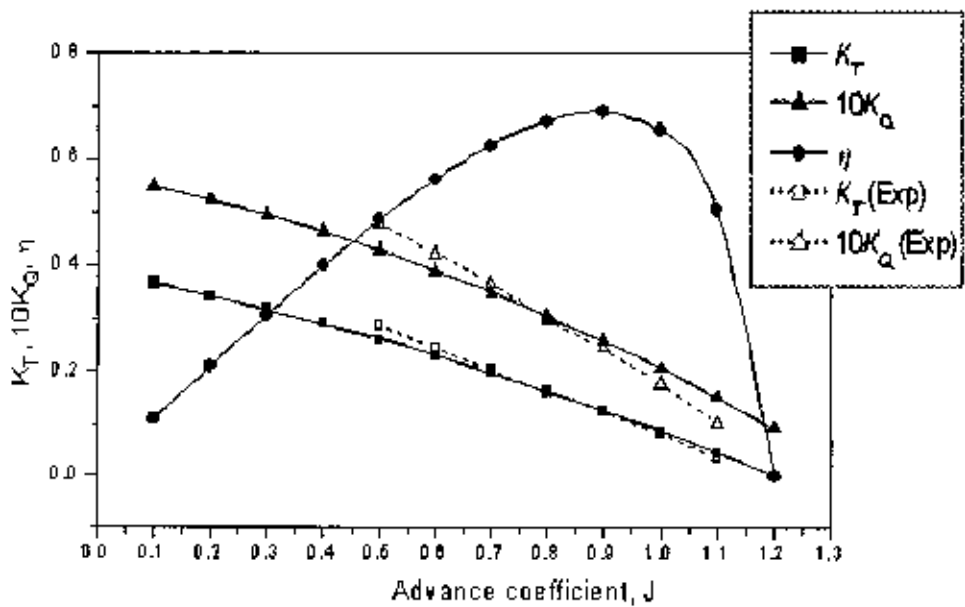
Figure 4.21: Comparison of open water hydrodynamic characteristics of DTRC4119 propeller with experimental values.

57

4.4.3. Comparison of Prediction Results with Experimental Measurements in case of Propeller with different hub taper angles.

The measurements consist of open water tests of five propellers with the same geometry (except hub taper angle). The model propellers have hub taper angles of 5°, 10°, 15°, 20° and 25° for pusher configurations. The sectional geometry of these propellers is given in Table A2.6-A2.7 and other geometric parameters are given in Table 4.3. A brief discussion of the measurements is given in [Islam et al., 2004]. The comparison is done for open water hydrodynamic characteristics of these two propellers (Prop. H15 and Prop. H20) in terms of thrust coefficient, K_T, and torque coefficient K_Q, propulsive efficiency, η for a wide range of advance coefficient, J. For the purpose of calculations the simulation parameters used are tabulated in Table 4.4.

Table 4.3: Geometric particulars of model propeller

Diameter (m)	0.27
Number of blade	4
Rotation (viewing at downstream)	Right hand
Design advance coefficient, J	0.8
Hub-Diameter (H/D) ratio	0.26 (based on regular straight hub)
Angular speed (rps)	15
Section thickness form	NACA 66 (DTMB Modified)
Section meanline	NACA = 0.8
Blade planform shape	Blade planform shape was based on David Taylor Model Basin model P4119 [Trouwborst,1998]
Expanded area ratio, EAR	0.60
Pitch distribution	Constant, $P/D = 1.0$
Skew distribution	Zero
Rake distribution	Zero

Table 4.4: Parameters used for prediction of hydrodynamic characteristics.

Simulation Parameter	Prop. H5, Prop. H10. Prop. H15, Prop. H20 & Prop. H25
Chordwise Grid Type	Uniform
Spanwise Grid Type	Uniform
No. of Panels Chordwise (blades)	9
No. of Panels Spanwise (blades)	8
Front Hub Cone Length	$0.20 \times D$
Rear Hub Cone Length	$0.21 \times D$
No. of Panels Axial (Front Hub)	7
No. of Panels Axial (Rear Hub)	9
No. of Panels Circular (Front Hub)	16
No. of Panels Circular (Rear Hub)	16
No. of Panels Between Blades	4
Hub Taper Angle	$5^\circ, 10^\circ, 15^\circ, 20^\circ$ & 25°
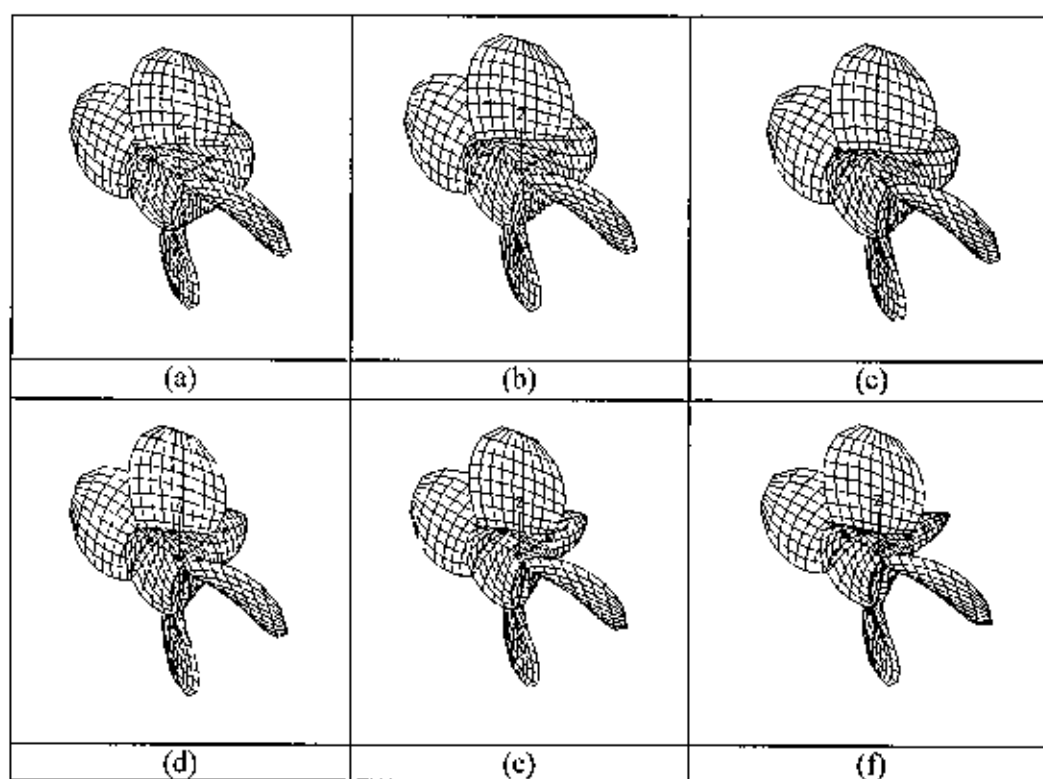
Figure 4.22: Mesh view of geometry of six model propellers. The propellers are termed as: (a) Straight hub propeller; (b) Prop. H5; (c) Prop. H10; (d) Prop. H15; (e) Prop. H20 and (f) Prop. H25.

Figure 4.22 shows the geometry of six propellers used for the study of hydrodynamic characteristics in open water conditions. A base model propeller with straight hub geometry is also shown in the Figure to depict the changes in hub geometry due to the taper angle. Figure 4.22(a) shows the propeller geometry in straight hub condition. Figures 4.22(b) , 4.22(c) , 4.22(d) , 4.22(e) and 4.22(f) show the geometries of propellers with positive hub taper angles (used in pusher configuration) 5° ,10° ,15° ,20° and 25°, respectively (termed as Prop. H5, Prop. H10, Prop. H15, Prop. H20 and Prop. H25 respectively).
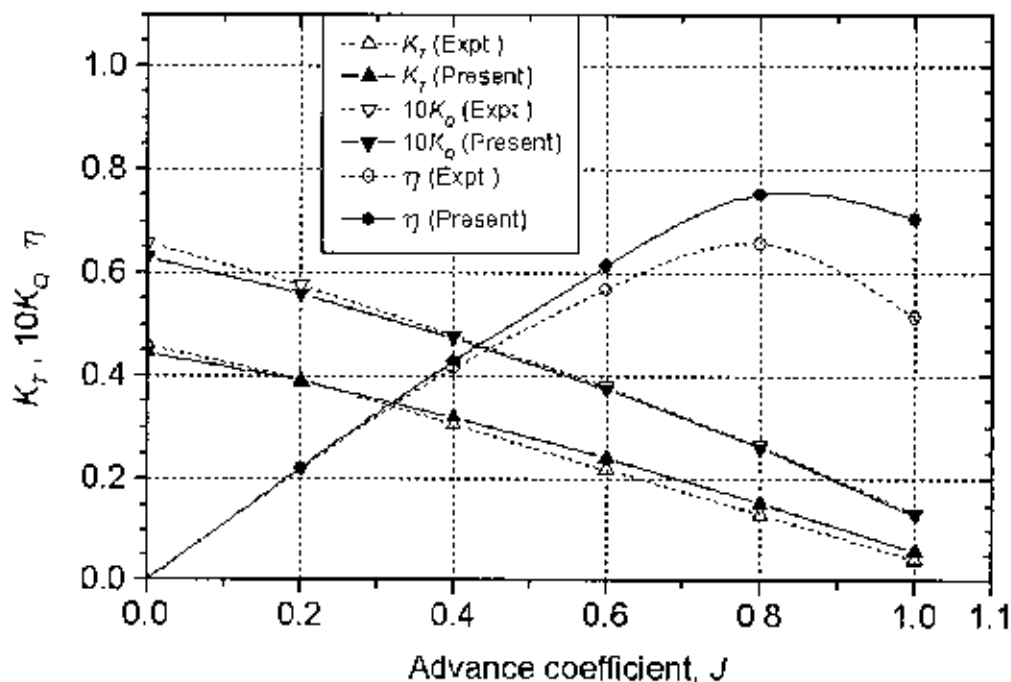
Figure 4.23: Comparison of predicted values of open water hydrodynamic characteristics with experimental measurements in case of propeller with hub taper angle of 15°.

The experimental results for the two propellers (Prop. H15 and Prop. H20) were collected and analyzed in terms of propeller thrust coefficient, K_T , propeller torque

coefficient, $10K_Q$, propulsive efficiency, η and propeller advance coefficient, J. Figures 4.23 and 4.24 shows comparison of predicted values of open water hydrodynamic characteristics with experimental measurements for model propeller Prop. H15 and Prop. H20 respectively. A discussion on the uncertainty of the experimental results is given in [Islam et al., 2004]. For predictions, uniform panel distributions are used in spanwise and chordwise directions.

It is seen that predictions of open water hydrodynamic characteristics are close to measurements for a wide range of advance coefficient. For thrust and torque coefficients, it is observed that the corresponding predicted values approach the measurements closely for a wide range of advance coefficient from bollard pull condition ($J = 0$) to advance coefficient, $J = 1.0$ (covers most of the operating range of any practical propeller). The predicted thrust is lower than that of the corresponding measured values for advance coefficients ($J = 0.0$-0.2) and higher for advance coefficients ($0.2<J<1.0$) corresponding to the measured values .The predicted torque is lower for advance coefficients ($J = 0.0$ – 0.2) and very much close for advance coefficients ($0.2<J<1.0$) corresponding to the measured values. This is true for both Prop. H15 and Prop. H20 (see Figure 4.23 and Figure 4.24).

Figure 4.24 shows comparisons of propeller open water hydrodynamic characteristics between experimental measurements and prediction for model propeller Prop. H20. The prediction is as good as for the case of Prop. H15. The only thing that should be mentioned here is that for lightly loaded conditions the over-estimation is of greater magnitude than that of Prop. H15. Because Prop. H20 has a larger hub taper angle, for

61

lightly loaded conditions the separation of flow occurs due to viscous effects over a larger hub area, resulting in a greater loss of torque
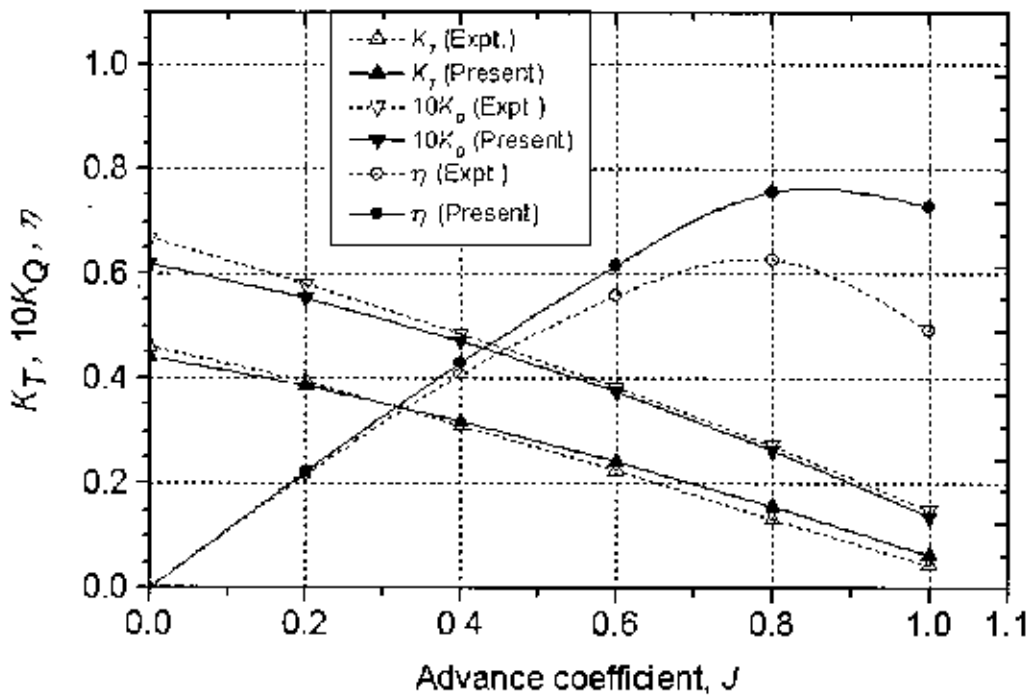
Figure 4.24: Comparison of predicted values of open water hydrodynamic characteristics with experimental measurements in case of propeller with hub taper angle of 20°.

4.4.4 Effects of Hub Taper Angle on Hydrodynamic Characteristics

The effects of hub taper angle on hydrodynamic characteristics of the model propellers are calculated in terms of thrust coefficient, K_T and torque coefficient, $10K_Q$ for a wide range of advance coefficient, J. The calculations are done for different hub taper angle 0°, 5°, 10°, 15°, 20° and 25°.

Table 4.5: Numerical results shows the effects of hub taper angle on the thrust coefficient of propellers with hub taper angle of 0°. 5°, 10°, 15°, 20° and 25°.

Advance coefficient, J	Thrust Coefficient, K_T					
	Hub taper angles					
	H0°	H5°	H10°	H15°	H20°	H25°
0.0	0.4608	0.4590	0.4557	0.4461	0.4427	0.4311
0.2	0.3947	0.3945	0.393	0.3905	0.3862	0.3788
0.4	0.3196	0.3211	0.3214	0.3207	0.3186	0.3151
0.6	0.2356	0.2387	0.241	0.2421	0.2422	0.2410
0.8	0.1427	0.1476	0.1517	0.1547	0.1571	0.1585
1.0	0.0409	0.0475	0.0536	0.0585	0.0632	0.0675

Table 4.6: Numerical results shows the effects of hub taper angle on the torque coefficient of propellers with hub taper angle of 0°, 5°, 10°, 15°, 20° and 25°.

Advance coefficient, J	Torque Coefficient, $10K_Q$					
	Hub taper angles					
	H0°	H5°	H10°	H15°	H20°	H25°
0.0	0.6434	0.6404	0.6355	0.6299	0.6185	0.6030
0.2	0.5668	0.5662	0.5638	0.5602	0.5543	0.5436
0.4	0.4750	0.4767	0.4769	0.4758	0.4726	0.4675
0.6	0.3860	0.3720	0.3748	0.3762	0.3760	0.3741
0.8	0.2457	0.2522	0.2577	0.2616	0.2645	0.2663
1.0	0.1083	0.1171	0.1255	0.1320	0.1382	0.1440

63

In Table 4.5 and Table 4.6 show the predicted thrust coefficient and torque coefficient of open water hydrodynamic characteristics for hub taper angles of 0°, 5°, 10°, 15°, 20° and 25° push configurations respectively. Hydrodynamic characteristics for a straight hub propeller are included in those figures to appreciate how the hub taper angles influence propulsive performance.

From Table 4.5 and Table 4.6, it is observed that the hub taper angle has more influence on K_T and K_Q at highly loaded conditions (low J values, $J <= 0.2$) and lightly loaded conditions (high J value, $J >= 0.8$) than for moderately loaded conditions ($0.2 < J < 0.8$). At $J = 0$, around 0.39% less thrust and 0.47% less torque ; around 1.11% less thrust and 1.23% less torque ; around 3.19% less thrust and 2.1% less torque ; around 3.93% less thrust and 3.87% less torque and around 6.45% less torque and around 6.28% less thrust produce for the propeller with 5° hub taper angle (i.e., Prop. H5); the propeller with 10° hub taper angle (i.e., Prop. H10); the propeller with 15° hub taper angle (i.e., Prop. H15); the propeller with 20° hub taper angle (i.e., Prop. H20) and the propeller with 25° hub taper angle (i.e., Prop. H25) respectively than that of straight hub propeller.

At design advance coefficient, $J = 0.8$, around 3.43% higher thrust and 2.65% higher torque; around 6.31% higher thrust and 4.88% higher torque; around 8.41% higher thrust and 6.47% higher torque ; around 10.09% higher thrust and 7.65% higher torque and around 11.07% higher thrust and 8.38% higher torque produce for the propeller with 5° hub taper angle (i.e., Prop. H5); the propeller with 10° hub taper angle (i.e., Prop. H10); the propeller with 15° hub taper angle (i.e., Prop. H15); the propeller with 20° hub taper angle (i.e., Prop. H20) and the propeller with 25° hub taper angle (i.e., Prop. H25) respectively than that of straight hub propeller. All numbers are in percentage based on straight hub propeller. From Table 4.5 and Table 4.6, it is also observed that if taper angle

64

increases, then thrust and torque coefficients decrease at lower advance coefficient and increase at higher advance coefficient.

The fact is that the majority of total thrust produced by the propeller blades is produced in the leading edge area. For propellers with positive taper hub angle some blade portion around the leading edge are chopped off and some blade portion around the trailing edge are added, resulting in lower total thrust and total torque produced by the propeller as compared to that of a straight hub propeller.

4.4.5 Effects of Pod-Strut Geometry on Hydrodynamic Characteristics

To study the effect of pod-strut geometry. the complete pod propulsion system, PPS (Propeller + Pod + Strut) has been analyzed by surface panel method. The effects of pod-strut geometry on propeller performance are analyzed by calculating the hydrodynamic characteristics of propeller when six pod-strut geometries are attached to it in pusher configurations. Here the six pod-strut bodies in push configurations are used with the parametric values tabulated in Table 4.7 .Here two of these pod-strut geometries (PS H15 and PS H20) are shown in figures as used by Islam (2004) for ease of comparison. The number of axial and circumferential panels for each pod is 14 and 16, respectively. The number of chord wise and span wise panels for the strut is 7 and 6, respectively. This results in the total number of panels on both pod-strut geometries equal to 308. The effect of pod-strut geometry on propeller performance is studied by calculating the hydrodynamic characteristics (in terms of thrust and torque coefficients and propulsive efficiency for a wide range of advance coefficient). Figure 4.27 and Figure 4.28 show the predictions of hydrodynamic characteristics of the model propellers when the pod-strut

65

geometries (PS H15 and PS H20) are attached to those in pusher configurations

Table 4.7: Geometric particulars of the pod–strut (PS) bodies

Parameters	PS H0, PS H5, PS H10, PS H15, PS H20 & PS H25
Pod Diameter	139 mm
Pod Length	410 mm
Strut Height	300 mm
Strut Chord Length	225 mm
Strut Distance	44 mm
Strut Width	60 mm
Fore Taper Length	85 mm
Fore Taper Angle	$0°, 5°, 10°, 15°, 20°$ & $25°$
Aft Taper Length	125 mm
Aft Taper Angle	$25°$
Fillets	50 mm
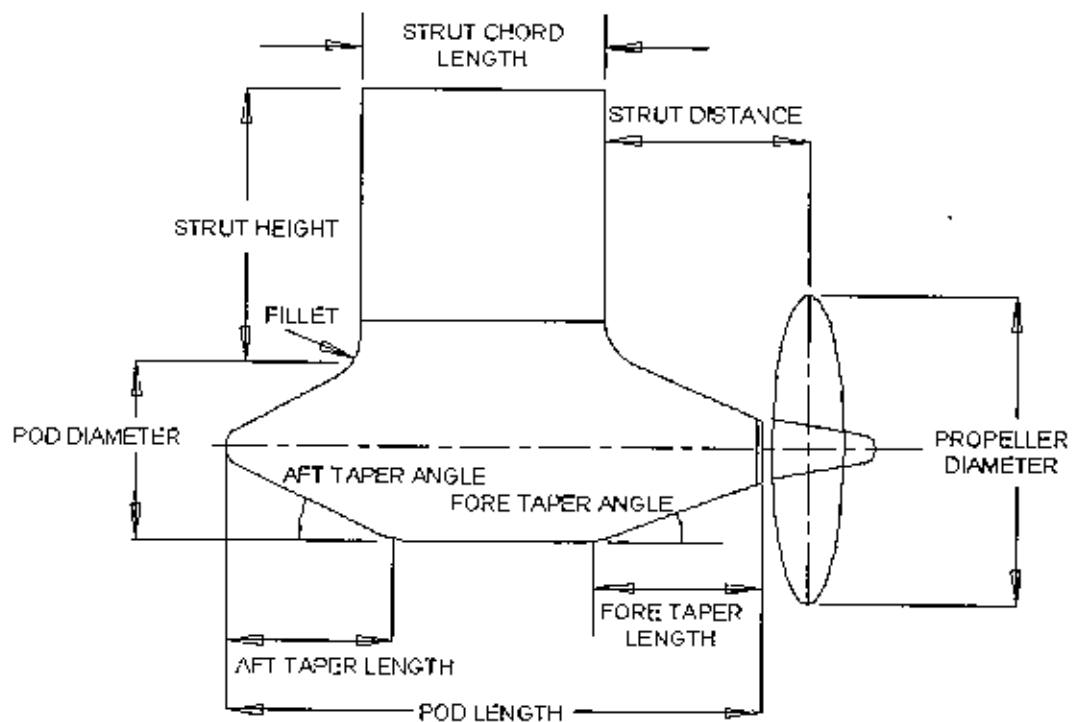
Figure 4.25: Geometric parameters used to define model pod geometry.
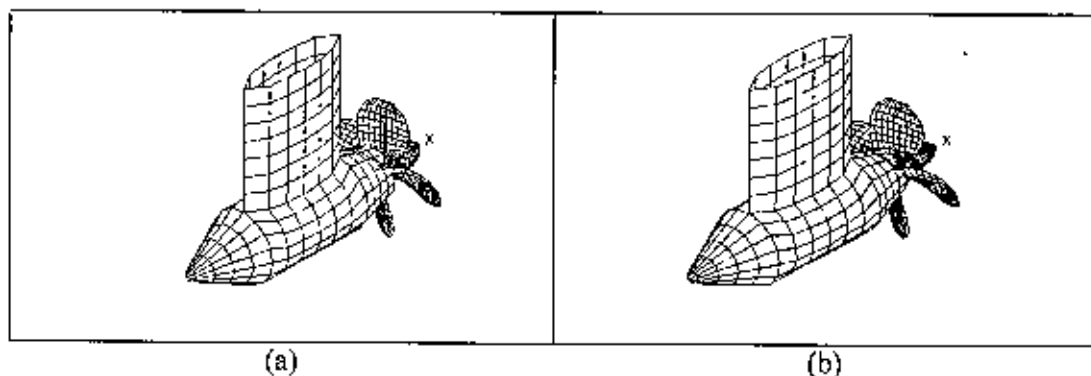
Figure 4.26: Mesh view of pod propulsion system (PPS) with (a) PS H15 and (b) PS H20

It can be seen from the figures that the thrust and torque of the propellers with pod-strut geometries in pusher configuration increase noticeably compared to the open propeller hydrodynamic characteristics. It is to be noted that only the hydrodynamic characteristics of the propeller is predicted in this research, in presence of pod- strut bodies.

Table 4.8: Quantitative study of effects of pod-strut geometry on hydrodynamic characteristics of the model propellers at bollard pull condition, $J = 0$ and design advance coefficient $J = 0.8$).

PS with hub taper angles	Thrust coefficient, K_T		Torque coefficient, $10K_Q$		Efficiency, h	
	Adv.coeff. $J = 0$	Adv.coeff. $J = 0.8$	Adv.coeff. $J = 0$	Adv.coeff. $J = 0.8$	Adv.coeff. $J = 0$	Adv.coeff. $J = 0.8$
PS H0	40.43%	76.45%	35.67%	64.22%	0%	7.44%
PS H5	38.34%	69.65%	33.87%	59.12%	0%	6.62%
PS H10	36.21%	63.68%	31.97%	54.44%	0%	6.00%
PS H15	35.78%	58.95%	30.15%	50.73%	0%	5.44%
PS H20	32.96%	54.42%	29.12%	47.18%	0%	4.97%
PS H25	32.29%	50.41%	28.79%	43.79%	0%	4.58%

67

Quantitatively, in the bollard pull condition (advance coefficient, $J = 0$) when PS H0; PS H5; PS H10; PS H15; PS H20 and PS H25 are attached to the Prop. H0; Prop. H5; Prop. H10; Prop. H15; Prop. H20 and Prop. H25 respectively in push configuration, increases of around 40.43% in thrust coefficient, 35.67% in torque coefficient and 0% in efficiency ; increases of around 38.34% in thrust coefficient, 33.87% in torque coefficient and 0% in efficiency; increases of around 36.21% in thrust coefficient, 31.97% in torque coefficient and 0% in efficiency; increases of around 35.78% in thrust coefficient, 30.15% in torque coefficient and 0% in efficiency; increases of around 32.96% in thrust coefficient, 29.12% in torque coefficient and 0% in efficiency and increases of around 32.29% in thrust coefficient, 28.79% in torque coefficient and 0% in efficiency respectively (as compared to those of the propellers in open water condition) are predicted. Again for PS H0; PS H5; PS H10; PS H15; PS H20 and PS H25 are attached to the Prop. H0; Prop. H5; Prop. H10; Prop. H15; Prop. H20 and Prop. H25 respectively in push configuration, increases of around 76.45% in thrust coefficient, 64.22% in torque coefficient and 7.44% in efficiency ; increases of around 69.65% in thrust coefficient, 59.12% in torque coefficient and 6.62% in efficiency; increases of around 63.68% in thrust coefficient, 54.44% in torque coefficient and 6% in efficiency; increases of around 58.95% in thrust coefficient, 50.73% in torque coefficient and 5.44% in efficiency; increases of around 54.42% in thrust coefficient, 47.18% in torque coefficient and 4.97% in efficiency and increases of around 50.41% in thrust coefficient, 43.79% in torque coefficient and 4.58% in efficiency (as compared to those of the propellers in open water condition) in the design advance coefficient, $J = 0.8$ are predicted respectively. All numbers in percentage are calculated by Equations (3.25), (3.26) and (3.27) .It is seen that, if the change in coefficients expressed in terms of percentage are decrease in both low and high advance coefficient with increase of hub taper angle.

68
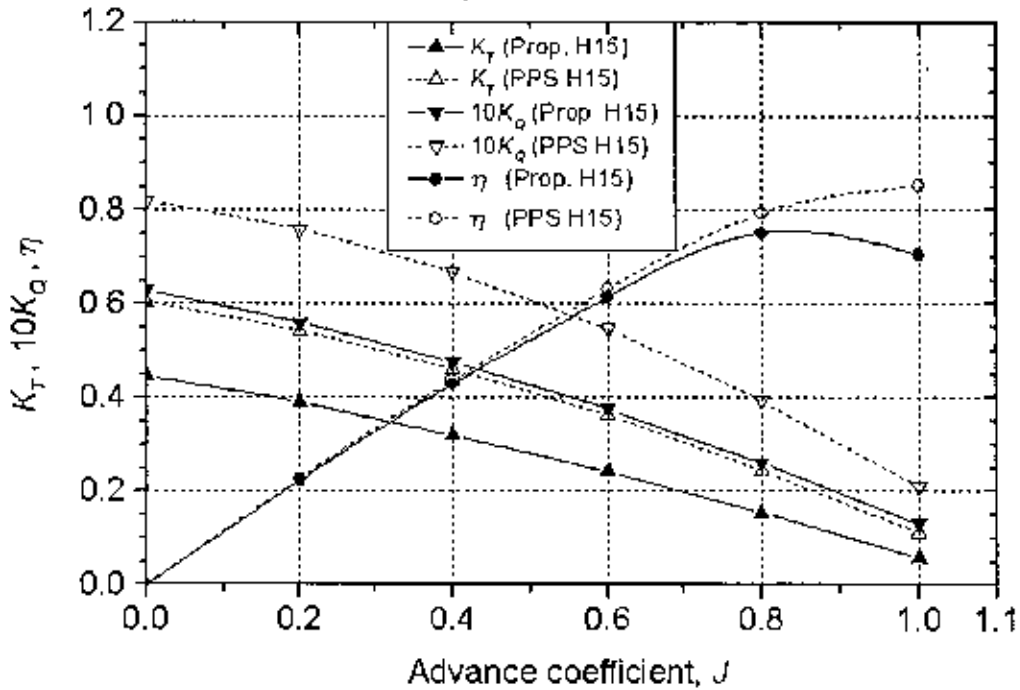
Figure 4.27: Numerical results showing the effect of pod-strut geometry on the hydrodynamic characteristics of propeller used in PPS H15.

The presence of the pod-strut geometry forward of the propeller acts as a blockage. In an earlier study of ice blockage effects [Veitch et al., 1997] and [Robbins et al.,1998], it is measured as well as predicted that the thrust and torque coefficients are apparently doubled due to the presence of an ice block (at a proximity of 1% radius of the propeller) forward of the propeller operating at an advance coefficient of $J = 0.4$. However, it must be remembered that in estimating the total thrust of the PPS (propeller with pod-strut), this increase in thrust of the propeller will not lead to an equivalent increase in PPS due to the thrust deduction effect between the propeller and the pod-strut and the drag of the pod-strut itself. No account is taken of the frictional wake (resulting in suction directed opposite to propeller thrust) from the pod-strut. A part of the estimated increase in thrust and torque of the propeller is due to this potential wake leading to an effective reduction in advance velocity of the propeller.

69
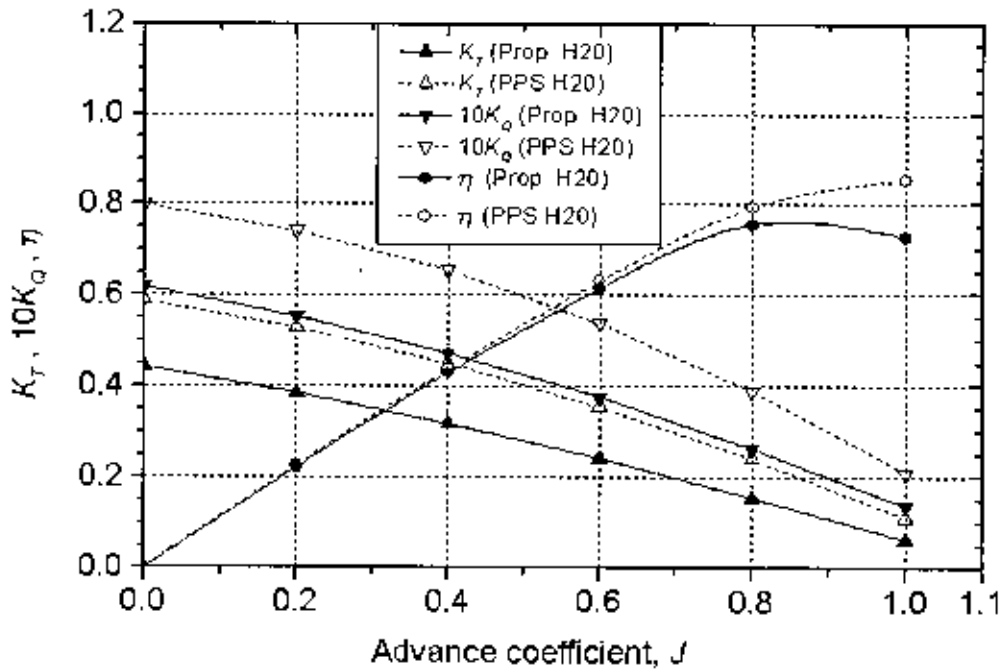
Figure 4.28: Numerical results showing the effect of pod-strut geometry on the hydrodynamic characteristics of propeller used in PPS H20.
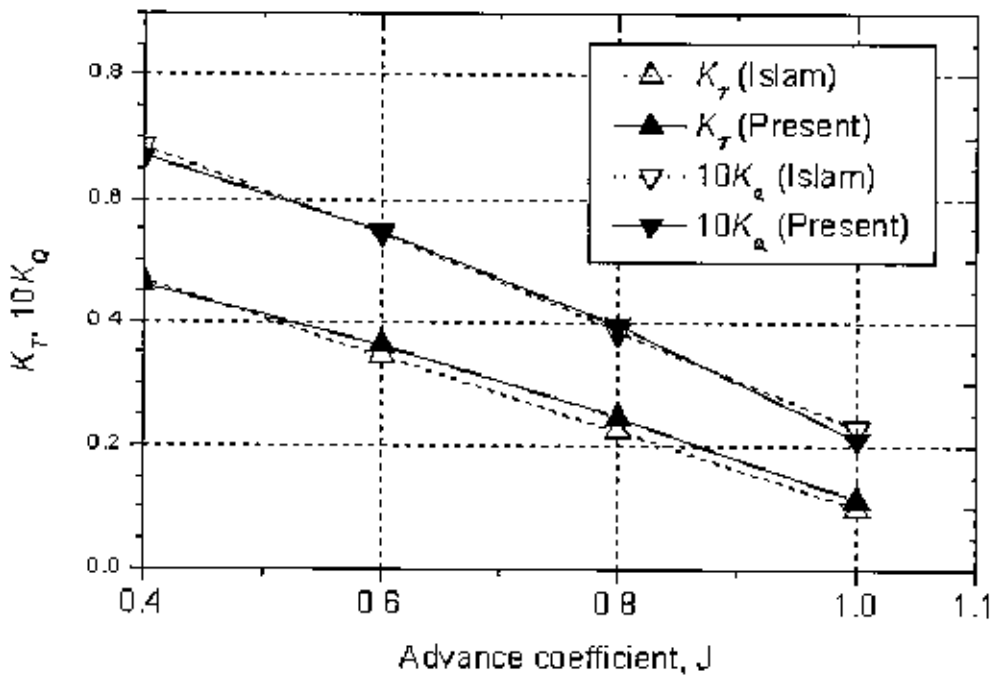
Figure 4.29: Comparison of the hydrodynamic characteristics of PPS H15.
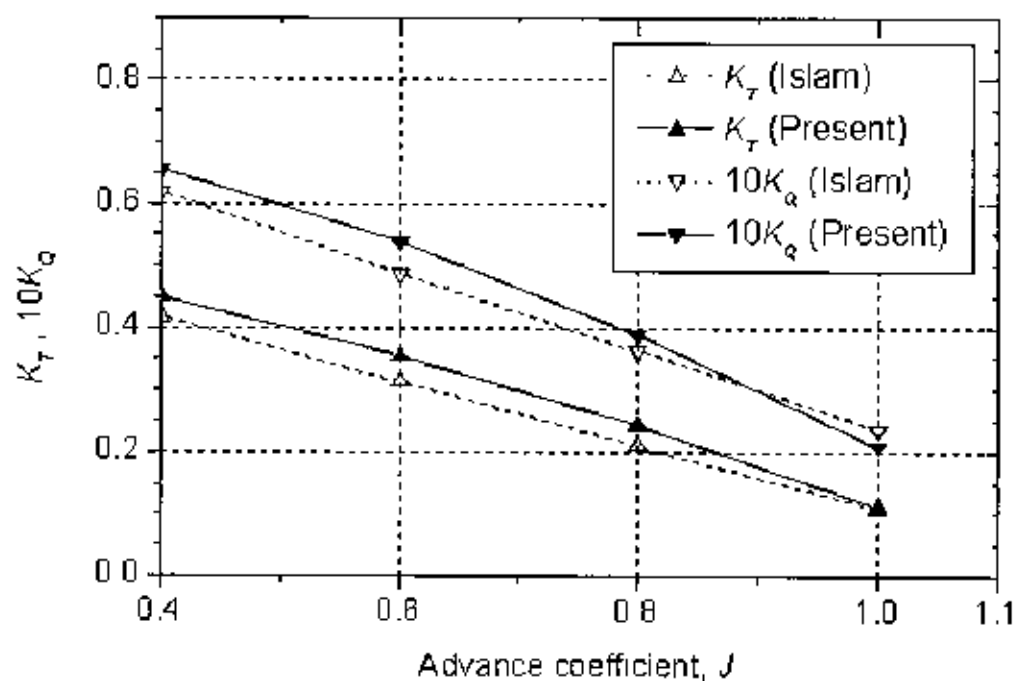
Figure 4.30: Comparison of the hydrodynamic characteristics of PPS H20.

CHAPTER 5

5. CONCLUSIONS AND RECOMMENDATIONS

5.1 Conclusion

A potential based surface panel method for computing hydrodynamic characteristics of modern marine propulsive device, i.e., podded propulsion system; PPS (propeller + pod + strut) operating in steady flow has been presented in this thesis. At first the method has been tested by applying it to isolated axi-symmetric underwater bodies (pod, submarine hull etc), strut and propeller and then combination of pod and strut and comparing predicted results with other published numerical/experimental results. From this study, following interesting conclusions can be drawn:

1. Results predicted by this method agree well with other published numerical/experimental results in case of isolated bodies, i.e., pod, strut, propeller etc. and combination of pod-strut geometry.

2. Reasonably good agreements between predictions and measurements for both propellers in pusher configurations are observed for a wide range of advance coefficient. The predicted values of thrust coefficient are lower than the corresponding measured values for lower advance coefficients ($J = 0.0\text{-}0.2$) and higher for higher advance coefficients ($0.2 < J < 1.0$). The predicted values of torque coefficients are lower for advance coefficients ($J = 0.0 - 0.2$) and very much close for advance coefficients ($0.2 < J < 1.0$).

3. Significant effects of hub taper angle on hydrodynamic characteristics of tapered hub propellers are observed. It is seen that hub taper angle has more influence on hydrodynamic characteristics at highly loaded conditions (low J value) than those at lightly loaded conditions (high J value). It is also seen that if taper angle increases, then thrust and torque coefficients decrease at low advance coefficient and increase at high advance coefficient.

4. Remarkable effects of pod-strut geometry on hydrodynamic characteristics of propeller are found in this research. It is observed that the thrust and torque of the propeller in presence of pod-strut geometries in pusher configuration have been increased up to about 32.29%-76.45% and 28.79%-64.22% respectively. The rate at which the thrust increases is greater than the rate at which the torque increases. As a result the efficiency of the propeller increases which is ranges from 4.58%-7.44% in this study. However, if the changes in coefficients for propeller with pod-strut geometry are expressed in terms of percentage with respect to propeller only, then they are decreased in both low and high advance coefficient with increase in hub taper angles.

5.2 Recommendations

In estimating hydrodynamic characteristics of the propeller used in PPS, losses due to frictional drag of the pod-strut geometry are not taken into account and effects of wake behind the pod-strut geometry are ignored. More study can be done to incorporate wake behind the pod and strut with this method.

The method is restricted only to analyze podded propulsion system without cavitation in this study. However, it can be extended to analyze podded propulsion system considering partial or super-cavitation on the propeller blades.

The method is restricted only to steady flow analysis. It can be extended to analyze unsteady flow around podded propulsion system.

The optimization problem can be solved incorporating optimization algorithm to the analysis method for design optimization of podded propulsion system.

References

Abbott. I. H. and Doenhoff. A.E.V., "Theory of wing section", Dover publication insurance. 1959.

Backlund, A. and Kuuskoski, J. "The contrarotating propeller (crp) concept with a podded drive", The Motor Ship Marine Propulsion Conference, Amsterdam, The Netherlands, March 2000.

Black, S. D., Chesnakas, C. J. and Jessup, S. D. "Investigation on efficiency improving boss-cap fins for t-ao 193". Tech. Rep. NSWCCD-50-TR-2001/067, Carderrock Division, Naval Surface Warfare Center, Naval Surface Warfare Center, Carderock Division, 9500 Macarthru Boulevard, West Methesda, MD 20817-5700, October 2001.

Bertin, J.J. and Smith, M.L.: Aerodynamics for engineers, Prentice Hall, 3rd .ed., 1997.

Bose, N.. Billet, M.. Anderson, P., Atlar, M., Dugue, C.. Ferrando, M., Qian. W., and Shen,Y., "Specialist committee on unconventional propulsors: Final report and recommendation to the 22nd International Towing Tank Conference", Tech. Rep., ITTC, USA, 1999.

Bose, N., "Ice blocked propeller performance prediction using a panel method", Tech. Rep. TR-HYD-95006. Memorial University of Newfoundland, Ocean Engineering Research Centre. Faculty of Engineering and Applied Science, Memorial University of Newfoundland, St. John's, NL. Canada, 1995.

Breslin, J.P. and Andersen, P.: Hydrodynamics of ship propellers, Cambridge University press, 1994.

Carlton, J. S., "Podded propulsors: Some design and service experience", The Motor Ship Marine Propulsion Conference, Copenhagen, Denmark, pp. 1-10, April 2002

Carlton, J. S.. Marine Propellers and Propulsion. Butterworth-Heinemann Ltd, 1994.

Cheng, B. H. , Dean J. S., and Cave, W. L. , "Hydrodynamic evaluation of hull forms with podded propulsors". Naval Engineers Journal, vol. 101, pp. 197-206, May 1989.

Chen, B. Y.-H. and Tseng, C. L.. "A contrarotating propeller design for a high speed patrol boat with pod propulsion", The Third International Conference on Fast Sea Transportation (FAST '95), Germany, pp. 1003-1013, July 1995.

Facinelli. W. A. and Muggeridge. D., "Integrated system analysis and design of podded ship propulsors", Journal of Marine Technology, vol. 35. no. 3, pp. 151-174. 1998

Funeno, I., "Hydrodynamic development of azimuthing podded propulsion system", Proceedings of the Kansai Society of Naval Architects, Japan, pp. 5-38, 2003.

Gupta. A., "Numerical prediction of flows around podded propulsors", Master's thesis, Departments of Civil Engineering, The University of Texas at Austin,2004.

Gindroz, B., Hoshino,T., Pylkkanen, J.V., eds., Proceedings of 22nd ITTC Propulsion Commitee Propeller RANS/PANEL Method Workshop Proceedings, Grenoble, France, Privately Printed, Val de Reuil, April 1998.

Han, J.-M., Paik, K.-J, Choi, S.-H. . Song, I.-H. and Shin, S.-C. , "Prediction of steady performance of podded propellers", Proceedings of Annual Spring Meeting of SNAK, Koje, Korea. pp. 144-147, April 2000.

Hess, J.L. and Smith, A.M.O., "Calculation of pPotential flow about arbitrary bodies", Progress in Aeronautical Science Series, Vol.8, pp1-137, Pergamon press, 1966.

Hess,J.L., "Panel Methods in Computational Fluid Dynamics", Annual Rev. Fluid Mech., vol.22,1990.

Hess, J. L. and Smith. A. M. O., "Calculation of nonlifting potential flow about arbitrary three-dimensional bodies", Journal of Ship Research, vol. 8, pp. 22-44, 1964.

Hoshino, T. and Nakamura. N., "Propeller design and analysis based on numerical lifting surface calculations". Marine and Offshore Computer Application, Springer-Verlag, Berlin, Germany, pp. 549-573, 1988.

Hoshino,T., "Hydrodynamics analysis of propeller in steady flow using a surface panel method 2nd report: Flow field around propeller", Journal of the Society of Naval Architectures of Japan, vol. 165, pp. 79-92, 1989.

Hoshino, T., "Hydrodynamics analysis of propeller in steady flow using a surface panel method", Journal of the Society of Naval Architects of Japan, vol. 165,pp. 55-70.

Hoshino, T., "Hydrodynamics analysis of propeller in unsteady flow using a surface panel method", Journal of the Society of Naval Architectures of Japan, vol. 174, pp. 71-87, 1993.

Halstensen, S. O., and Leivdal, P. A.,"The development of the speedz propulsion system", Proceedings of 7th International High Speed Surface Craft Conference, January 1990.

Islam M.F., "Numerical investigation on effects of hub taper angle and pod-strut geometry on propulsive performance of pusher propeller configurations", Master of Engineering thesis, Memorial University of Newfoundland. Canada, 136p. 2004.

Islam M., Taylor. R., Quinton, J., Veitch, B., Bose, N., Colbourne, B., and Liu, P., "Numerical investigation of propulsive characteristics of podded propellers". Proceedings of the 1st International Conference on Technological Advances in Podded Propulsion, School of Marine Science and Technology, University of Newcastle, UK, April pp. 513-525. 2004.

Islam M., Veitch,B., Bose, N. and Liu, P., "Numerical study of hub taper angle on podded propeller performance", Journal of Marine Technology, Vo 43, No.1, pp. 1-10.,2006

Karim, M.M., Hakim, M.A. and Hasan, M.K., "A study of surface panel method for the analysis of Marine Propellers in steady flow", Journal of Mechanical Engineering, vol.ME35, pp 42-54, June 2006,

Kawakita, C. Hoshino, T. and Minamiura, J., "Prediction of hydrodynamic performance of hydrofoil, strut and pod configuration by a surface panel method", Journal of Seibu Sosen Kai, vol. 6, no. 87, pp. 15-25, 1994.

Kim, H. and Kim, D., "Computational study on propulsive characteristics of tractor and pusher type podded propellers", Proceedings of Annual Spring Meeting of SNAK, Koje, Korea, pp. 161-164, April 2001.

Kurimo, R., "Sea trial experience of the first passenger cruiser with podded propulsors", Proceedings of the 7th Int. Symposium on Practical Design of Ships and Mobile units (PRADS), pp. 743-748, 1998.

Karafiath, G. and Lyons, D., "Hydrodynamic performance with pod propulsion", Proceedings of twenty fifth American Towing Tank Conference, Iowa, USA, pp. 3.7-3.23, September 1998.

Karafiath, G. and Lyons, D., "Pod propulsion hydrodynamics-US Navy experience", Proceedings of the Fifth International Conference on Fast Sea Transportation (FAST '99), Seattle, USA, pp. 119-135, July 1999.

Kerwin, J. E., Kinnas,S. A. and Lee, J. T., "A surface panel method for the hydrodynamic analysis of ducted propellers", SNAME Transactions, vol. 95, pp. 93-122, 1987.

Kron, P. and Holmstrom, L. "Hydrodynamic aspects of Mermaid^{TM} propulsion system", 21st Century Cruise Ship: London Conference and Symposia, Vol.111, No. 3, Part 1, Session 1, pp. 1-12, April 1999.

Kim. S.-E. and Choi. S.-H., "Model tests on propulsion systems for ultra large container vessel", Proceedings of the Twelfth International Offshore and Polar Engineering Conference, Kitakyushu, Japan, pp. 520-524, May 2002.

Lavini, G., "New hull and propeller design for twin screw ships with electric pod drive", Proceedings of NAV 2000: International Conference on Ship and Shipping Research, Venice, Italy, pp. 6.6.1-6.6.12, September 1990.

Laukia, K., "The Azipod system-operational experience and designs for the future", Redundancy vs. Reliability: The Motor Ship, 18th Annual Marine propulsion Conference. Radisson Sas Hotel, Hamburg. Germany, pp. 77-94, March 1996.

Lepeix, R., "Hydrodynamic trends in hull lines of podded driven large cruise vessels", Proceedings of the Conference on Practical Designs of Ships and Other Floating Structures (PRADS) 2001, Shanghai, China, pp. 767-776. September 2001.

Liu, P., "Software development on propeller geometry input processing and panel method predictions on propulsive performance of the r-class propeller",Tech. Report, MMC Engineering and Research, Burin Bay Arm, NL, Canada, September 1996

Liu, P., A time-domain panel method for oscillating propulsors with both chord-wise and spanwise fleexibility. Ph.D thesis, Memorial University of Newfoundland, April 1996.

Morino, L., Chen, L. T., and Suciu, E. O., "Steady and oscillatory subsonic and supersonic aerodynamics around complex configurations", AIAA Journal, vol. 13, no. 3, pp. 368-374. 1975.

Mewis, F., "The efficiency of pod propulsion", Proceedings of HADMAR 2001, pp. 1-12, October 2001.

Niini, M., "Azipod propulsion breakthrough for large cruise ships", Proceedings of the Conference Cruise+Ferry'97, London, UK, p. 14 pages, 1997.

Newman. J. N., "Distributions of sources and normal dipoles over a quadrilateral panel", Journal of Engineering Mathematics, vol. 20, pp. 113-126, 1986

Nocod, J.-P. and Simon, P., "A Step ahead in electric propulsion with Mermaid^{TM}", All Electric Ship: Developing Benefits for Maritime Applications. pp. 219-221, 1998.

79

Ouchi, K.. "Research and development of pbcf to enhance propeller efficiency", Proceedings of the Tenth Motor Ship International Marine Propulsion Conference, London, UK, March 1988.

Paik, K.-J., Han, J.-M. , Lee, Y.-C., Shin. S.-S. and Song, J.-H., "Numerical study on the contra-rotating propeller using the podded propeller", Proceedings of Annual Spring Meeting of SNAK, Koje, Korea, pp. 195-198, April 2002.

Pustoshny, A. V. and Kaprantsev, S. V. "Azipod propeller blade cavitation observations during ship maneuvering", Proceedings CAV 2001: Fourth International Symposium on Cavitation. California Institute of Technology, Pasadena, CA USA, pp. 1-8, 2001.

Rains, D. A. and. Vanlandingham, D. J., "Hydrodynamics of podded ship propulsion", Journal of Hydronautics, vol. 14, no. 1-4, pp. 18-24, 1981.

Raynor, S. J., "The benefits of podded propulsion in the offshore market", Proceedings of the Dynamic Positioning Conference: Thrusters and Drive Systems, Houston, TX, USA, pp. 1-11, October 1998.

Robbins, I., Doucet, J. M. . Liu, P., Bose, N., "Numerical prediction of ice-induced loads on ice-class screw propellers: Hydrodynamic loads due to blockage", Tech. Rep. OERC-1998-003, Ocean Engineering Research Center and Institute for Marine Dynamics, National Research Council, St. John's, NL, Canada, April 1998.

Sohaib, M.. Ayub, M. and Rafique, M., "computational cavitation analysis of submerged body at different depths", Proceedings of the European Conference on Computational Fluid Dynamics, ECOMAS CFD, Netherlands, 2006.

Suciu, E. O. and Morino, L., "A nonlinear finite-element analysis of wings in steady incompressible flows with wake roll-up", AIAA page no 64-76., AIAA 14th Aerospace Science Meeting. Washington, D.C, 1976.

Szantyr, J.A.. "A surface panel method for hydrodynamic analysis of pod propulsors", Marine Technology Transactions, vol. 12, p. 20 pages, 2001

80

Szantyr, J, "Hydrodynamic model experiments with pod propulsors", Ocean Engineering International. 5(2):pp. 95-103, 2001.

Terwisga,T.V., Quadvlieg, F., and Valkhof, H., "Steerable propulsion units: Hydrodynamic issues and design consequences", 80th anniversary of Schottel GmbH & Co., 2001.

Toxopeus. S. and Loeff, G., "Manoeuvring aspects of fast ships with pods", Euro Conference on High-Performance Marine Vehicles HIPER'02. Bergen, pp. 392-406, September 2002.

Triantafyllou, M., Hover, F. and Stettler, J. "System dynamics and control of podded propulsors". 1st year Report, Dept. of Ocean Engg., MIT, 2003.

Trouwborst, W., "Non-conventional ship propulsion: Literature study on contra rotating propellers and podded propulsion", Tech. Rep. TNO-Rep. 98-CMC-R1337, TNO Building and Construction Research, Delft, The Netherlands, June 1998.

Trägårdh, P., Lindell, P. and Sasaki, N., "Double acting tanker-experience from model tests and sea trials", Proceedings of the 1st International Conference on Technological Advances in Podded Propulsion, School of Marine Science and Technology, University of Newcastle, Newcastle, UK, p. 14 pages, April 2004.

Veitch. B., Bose, N., Meade, C., and Liu, P., "Predictions of hydrodynamic and ice contact loads on ice-class screw propellers", Proceedings of the 16th international Conference on Offshore Mechanics and Arctic Engineering, pp. 119-125, 1997

Yanagizawa, M. "Calculation for aerodynamics characteristics on a 3-D lifting body in subsonic flow using boundary element method", Technical report on National Aerospace Laboratory. TR-835, September, 1984.

81

Appendix 1

A.1: Influence Coefficients

Using the local coordinate system (ξ, η) and the position vector Q_i $(i=1\sim4)$ of four corner points of a quadrilateral hyperboloidal panel, any position vector $Q(\xi, \eta)$ on the panel can be expressed as:

$$Q(\xi,\eta) = \sum_{i=1}^{4} \alpha_i Q_i \qquad (A.1.1)$$

Where, α_i is the interpolation functions defined by

$$\alpha_i = \frac{1}{4}(1 + \xi_i \xi)(1 + \eta_i \eta) \qquad (A.1.2)$$

Where, $-1 \le \xi \le 1, -1 \le \eta \le 1$

Therefore the arbitrary quadrilateral hyperboloidal panel in a global coordinate system corresponds to a square in the local coordinate system as shown in Figure. A.1.1
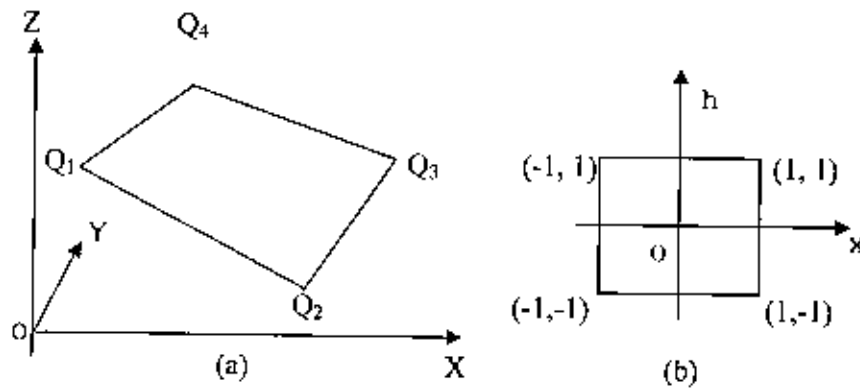
Figure A.1.1: Definition of hyperbolodial panel in global (a) and local (b) coordinate system.

If two vectors a_1, a_2 tangent to the surface is defined by the following relationship:

$$a_1 = (\xi,\eta) = \frac{\partial Q}{\partial \xi}, \qquad a_2 = (\xi,\eta) = \frac{\partial Q}{\partial \eta} \qquad (A.1.3)$$

the unit normal vector can be given by:

82

$$n(\xi,\eta) = \frac{a_1 \times a_2}{|a_1 \times a_2|} \tag{A.1.4}$$

and the surface element can be expressed as:

$$ds = |a_1 \times a_2|\, d\xi\, d\eta \tag{A.1.5}$$

Then, all the integrals, which appeared in the influence coefficients, can be written as the form of :

$$I = \int\limits_{\eta=-1}^{1} \int\limits_{\xi=-1}^{1} f(\xi,\eta)\, d\xi\, d\eta \tag{A.1.6}$$

if the integrand $f(\xi,\eta)$ is expressed as:

$$f(\xi,\eta) = \frac{\partial^2 F(\xi,\eta)}{\partial \xi\, \partial \eta} \tag{A.1.7}$$

then the following relation can be obtained:

$$I = F(1,1) - F(1,-1) - F(-1,1) + F(-1,-1) \tag{A.1.8}$$

Thus the influenced coefficients C_{ij} and B_{ij} are evaluated analytically [Suciu and Morino, 1976] as:

$$C_{ij} = I_D(1,1) - I_D(1,-1) - I_D(-1,1) + I_D(-1,-1) \tag{A.1.9}$$

$$B_{ij} = I_S(1,1) - I_S(1,-1) - I_S(-1,1) + I_S(-1,-1) \tag{A.1.10}$$

where .

$$I_D(\xi,\eta) = \frac{1}{2\pi} \tan^{-1}\left(\frac{(R \times a_1) \bullet (R \times a_2)}{|R| R \bullet (a_1 \times a_2)} \right) ; \tag{A.1.11}$$

$$I_S(\xi,\eta) = -\frac{1}{2\pi} \left\{ -\frac{(R \times a_1) \bullet n}{|a_1|} \sin^{-1}\left(\frac{(R \bullet a_1)}{|R \times a_1|} \right) + \frac{(R \times a_2) \bullet n}{|a_2|} \sin^{-1}\left(\frac{(R \bullet a_2)}{|R \times a_2|} \right) \right\}$$
$$- R \bullet n I_D(\xi,\eta) \tag{A.1.12}$$

and $\quad R = Q(\xi,\eta) - P_i$

Appendix 2

Table A2.1: Geometry of Pod A

X	R
-0.4	0.016
-0.2888889	0.10178928
-0.17777778	0.1859307
-0.06666666	0.25559401
0.04444444	0.30926707
0.15555558	0.35071787
0.26666668	0.3811607
0.37777778	0.40088868
0.4888889	0.41221717
0.6	0.41596502
0.6222789	0.416
0.6873106	0.416
0.789882663	0.416
0.92152184	0.416
1.0717269	0.416
1.2282733	0.416
1.3784784	0.416
1.5101736	0.416
1.6126895	0.416
1.6777213	0.416
1.7	0.4159999
1.7996619	0.41271626
1.8993238	0.40193957
1.9989856	0.3824254
2.0986475	0.35273554
2.1983094	0.31150802
2.2979712	0.25735408
2.397633	0.1888398
2.4972951	0.104824535

2.596957	3.384173E-3

Table A2.2: Geometry of the DARPA2 submarine hull

X	R
0	0.005
0.3	0.445992237
0.6	0.56368458
0.9	0.631015523
1.2	0.678895481
1.5	0.718572558
1.8	0.753605921
2.1	0.783877981
2.4	0.807812234
2.7	0.82386672
3.0	0.831701435
3.3	0.833331415
3.535	0.833333
3.8225	0.833333
4.31	0.833333
4.7975	0.833333
5.285	0.833333
5.7725	0.833333
6.26	0.833333
6.7475	0.833333
7.235	0.833333
7.7225	0.833333
8.21	0.833333
8.6975	0.833333
9.185	0.833333
9.6725	0.833333
10.16	0.833333
10.6475	0.833333

10.648	0.833333425
10.98116667	0.828267281
11.31433334	0.800694854
11.64750001	0.743917178
11.98066668	0.660366099
12.31383335	0.556846005
12.64700002	0.442250852
12.98016669	0.326435892
13.31333336	0.219824397
13.64650003	0.135118772
13.9797	0.097916667
13.9796667	0.097916524
14.0420934	0.095910951
14.1044868	0.089698248
14.1668802	0.078283084
14.2292736	0.058705255
14.291667	0.001

Table A2.3: Geometry of strut with NACA0012 section

X	R
0	0
0.0023342	0.0084289
0.0093149	0.0164706
0.0208771	0.0240706
0.0369127	0.0311559
0.0465628	0.0344792
0.057272	0.0376414
0.0817649	0.0434371
0.1101628	0.0484567
0.1422005	0.0526251
0.1775789	0.0558856

0.2159676	0.0582048
0.2570083	0.0595755
0.3003177	0.0600172
0.3454915	0.0595747
0.3921079	0.0583145
0 4397317	0.05632
0.4879181	0.0536866
0.5362174	0.0505161
0.5841786	0.0469124
0.6313537	0.0429778
0.6773025	0.0388109
0.7215958	0.0345058
0.7638202	0.0301515
0.8035813	0.0258337
0.8405079	0.0216347
0.8742554	0.0176353
0.9045085	0.0139143
0.9309849	0.0105485
0.9534372	0.0076108
0.9716559	0.0051685
0.9854709	0.0032804
0.9947532	0.0019938
0.9994161	0.0013419
1.0	0

Table A2.4: Geometry of Pod B as used by Szantry (2001)

X	R
-2.265	0.02
-2.0800001	0.16028973
-1.8950001	0.22174709
-1.71	0.26552885

-1.5250001	0.29938104
-1.34	0.32648843
-1.155	0.34837907
-0.97	0.36596354
-0.78499996	0.37985682
-0.6	0.3904801
-0.57569575	0.39166897
-0.50475215	0.39478877
-0.39291644	0.39880946
-0.24924898	0.40249016
-0.0853889	0.40468
0.08538896	0.40468
0.2492491	0.4024901
0.39291653	0.39880943
0.50475215	0.3947888
0.5756959	0.391669
0.6	0.3904801
0.785	0.37985682
0.97	0.36596357
1.1550001	0.34837904
1.3400002	0.3264884
1.5250001	0.29938104
1.7100002	0.26552876
1.8950001	0.22174709
2.0800001	0.16029005
2.265	0.02

Table A2.5: Geometry of the strut having NACA066section with leading edge at the location X=-0.6 on Pod B and trailing edge at X=+0.6

X	Y	Z
-0.6	1.54	0.0E+0
-0.5756959	1.54	-0.068673864

-0.50475215	1.54	-0.13486163
-0.39291653	1.54	-0.19476245
-0.2492491	1.54	-0.23895688
-0.08538896	1.54	-0.2590484
0.0853889	1.54	-0.2476123
0.24924898	1.54	-0.20349935
0.39291644	1.54	-0.13812754
0.50475215	1.54	-0.070037215
0.57569575	1.54	-0.018887708
0.6	1.54	0.0E+0

Table A2.6: Sectional geometry offsets for the model propeller in the radial direction [Here r is local radius. R is the propeller radius, D is the propeller diameter C is local chord length, P local pitch, α is local skew angle, β is local rake angle, t_{max} local maximum thickness and f_{max} is local maximum camber as used by Islam (2004)]

r/R	C/D	P/D	α	β	t_{max}/C	f_{max}/C
0.30	0.285550	1.00	0.00	0.00	0.15530	0.02318
0.40	0.318870	1.00	0.00	0.00	0.11800	.0.03303
0.50	0.345968	1.00	0.00	0.00	0.09160	0.02182
0.60	0.363140	1.00	0.00	0.00	0.06960	0.02072
0.70	0.342423	1.00	0.00	0.00	0.04206	0.02003
0.80	0.284605	1.00	0.00	0.00	0.03321	0.01967
0.90	0.218593	1.00	0.00	0.00	0.03228	0.01817
0.100	0.126036	1.00	0.00	0.00	0.03160	0.01631

Table A2.7: Model propeller sectional maximum thickness and camber distribution.
[x/C is the normalized distance from leading edge; t/C is sectional thickness and f/C is sectional camber. All values are normalized by local chord length, C as used by Islam (2004)]

x/C	t/C	f/C
0.0000	0.0000	0.0000
0.0125	0.2088	0.0907
0.0250	0.2932	0.1586
0.0500	0.4132	0.2712
0.0750	0.5050	0.3657
0.1000	0.5814	0.4482
0.1500	0.7042	0.5869
0.2000	0.8000	0.6993
0.3000	0.9274	0.8635
0.4000	0.9904	0.9615
0.4500	1.0000	0.9881
0.5000	0.9924	1.0000
0.6000	0.9306	0.9786
0.7000	0.8070	0.8892
0.8000	0.6220	0.7027
0.9000	0.3754	0.3586
0.9500	0.2286	0.1713
1.0000	0.0666	0.0000

Appendix 3

DEFINITION OF SOME RELATED TERMS

Propeller: Propeller is a type of fan which transmits power by converting rotational motion into thrust. It can be used to drive an aircraft, ship etc.. It consists of one or more blades about a central shaft and operates like a rotating screw or wing. A pressure difference between the forward and rear surfaces of the airfoil-shaped blade is produced and air or water accelerated behind the blade(See Figure 4.9).

Hub: The hub of a propeller is the solid center disk that matches with the propeller shaft and to which the blades are attached. Ideally the hub should be as small in diameter as possible to obtain maximum thrust, however there is a tradeoff between size and strength. Too small a hub ultimately will not be strong enough (See Figure 4.9).

Pod: A pod is a cylindrical shape used in podded propulsion system. In push type podded propeller it is in front of the propeller and in pull type podded propeller it is behind the propeller (See Figure 2.2).

Strut: A strut is a structural component to hold the pod propeller with ship hull (See Figure 2.2).

Blades: Twisted fins or foils that protrude from the propeller hub. The shape of the blades and the speed at which they are driven dictates the thrust a given propeller can deliver (See Figure 4.9).

91

Blade Root and Blade Tip: The root of a propeller blade is where the blade is attached to the hub. The tip is the outermost edge of the blade at a point furthest from the propeller shaft (See Figure 4.9).

Blade Face and Back: The face of a blade is considered to be the high-pressure side, or pressure face of the blade. This is the side that faces aft (backwards) and pushes the water when the vessel is in forward motion. The back of the blade is the low pressure side or the suction face of the blade. This is the side that faces upstream or towards the front of the vessel (See Figure 4.9).

Leading and Trailing Edges: The leading edge of a propeller blade or any foil is the side that cuts through the fluid. The trailing edge is the downstream edge of the foil (See Figure 4.9).

Right Handed vs. Left Handed: A propeller's "handedness" affects its shape. A right-handed propeller rotates clockwise when propelling a vessel forward, as viewed from the stern of the ship. A left-handed propeller rotates counter-clockwise, as viewed from the stern, when in a forward propulsion mode. When viewing a propeller from astern, the leading edges of the blades will always be farther away from you than the trailing edges. The propeller rotates clockwise, and is right-handed, if the leading edges are on the right. A propeller's handedness is fixed. A right-handed propeller can never be exchanged with a left handed propeller, and vice versa.

Pitch: The pitch of a propeller is defined similarly to that of a wood or machine screw. It indicates the distance the propeller would "drive forward" for each full rotation.

Propeller section: A circular arc section cut through the blade at some radius. When this section is "flattened out" it looks like a foil section (See Figure 4.11).

Meanline: Half distance along a section between the upper and lower surfaces of the blade(See Figure 4.11).

Nose-Tail line: Straight line connecting the leading edge meanline point to the trailing edge meanline point (See Figure 4.11).

Chordlength: Length of Nose-tail line (See Figure 4.11).

Camber height: Distance between nose-tail line and meanline normal to the nose-tail line (varies with chordwise position) (See Figure 4.11).

Thickness: Section thickness along a line normal to the meanline. Varies with chordwise position (See Figure 4.11).

Midchord line: Line produced from the midchords (i.e. Midpoint of section nose tail line) of each section along a propeller blade (See Figure 4.11).

Rake: Axial distance from the midchord point at the hub section and the section of interest (See Figure 4.10).

Skew or Skew Angle: Tangential component of the angle formed on the propeller between a radial line going through the hub section midchord point and a radial line going through the midchord of the section of interest and projected (See Figure 4.10).